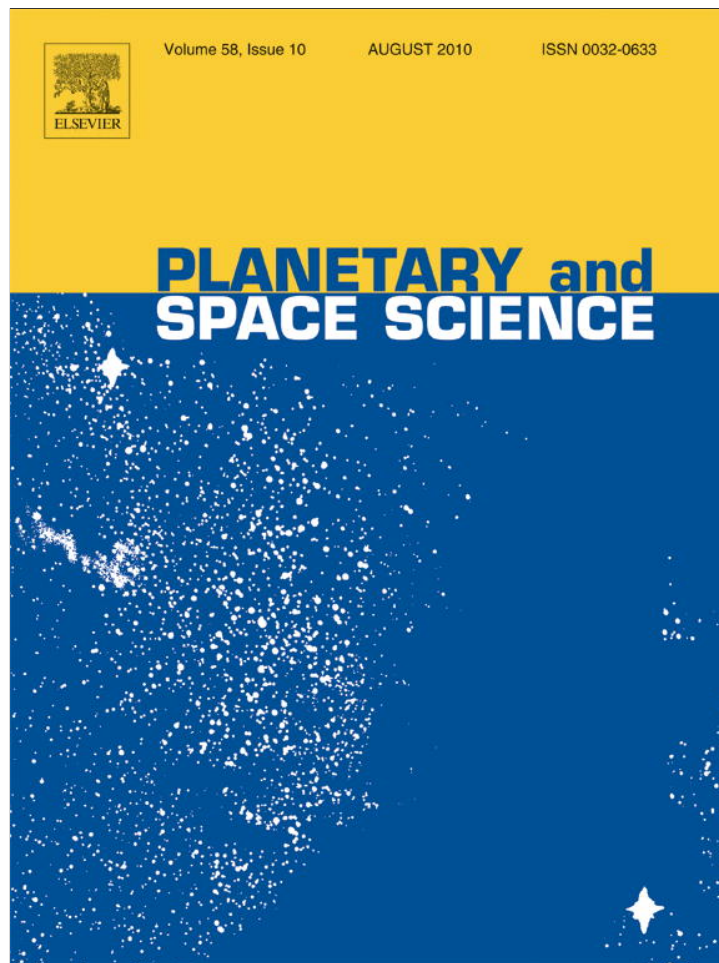


Provided for non-commercial research and education use.
Not for reproduction, distribution or commercial use.



This article appeared in a journal published by Elsevier. The attached copy is furnished to the author for internal non-commercial research and education use, including for instruction at the authors institution and sharing with colleagues.

Other uses, including reproduction and distribution, or selling or licensing copies, or posting to personal, institutional or third party websites are prohibited.

In most cases authors are permitted to post their version of the article (e.g. in Word or Tex form) to their personal website or institutional repository. Authors requiring further information regarding Elsevier's archiving and manuscript policies are encouraged to visit:

<http://www.elsevier.com/copyright>



Contents lists available at ScienceDirect

Planetary and Space Science

journal homepage: www.elsevier.com/locate/pss

UVolution: Compared photochemistry of prebiotic organic compounds in low Earth orbit and in the laboratory

Yuan Yong Guan^a, Nicolas Fray^a, Patrice Coll^a, Frédérique Macari^a, Didier Chaput^b, François Raulin^a, Hervé Cottin^{a,*}

^a LISA, UMR CNRS 7583, Université Paris-Est Créteil et Université Paris Diderot, Institut Pierre Simon Laplace, CMC, 61 Avenue du Général de Gaulle, 94010 Créteil Cédex, France

^b CNES, Centre spatial de Toulouse, 18 Avenue Edouard Belin, 31401 Toulouse Cedex 9, France

ARTICLE INFO

Article history:

Received 2 February 2010

Received in revised form

8 May 2010

Accepted 25 May 2010

Available online 9 June 2010

Keywords:

Astrobiology

VUV

Organic matter

Photolysis

Low Earth Orbit exposure

Biopan

ABSTRACT

Solar UV radiation is a major source of energy for chemical evolution of organic materials in the Solar System. Therefore studies on the photostability of organic compounds in extraterrestrial environments are of prime importance for the understanding of the extraterrestrial origin of organic materials on Earth. A series of organic samples have been photolysed in Earth orbit during the ESA BIOPAN 6 mission (14–26/09/2007). Their photochemical lifetime has been measured and compared to results recorded in the laboratory using a lamp that simulates the solar radiation in the VUV domain. The half-lives at a distance of 1 AU from the Sun have been measured for glycine, xanthine, hypoxanthine, adenine, guanine, urea, carbon suboxide polymer ((C₃O₂)_n) and HCN polymer. They range from a few days to a lower limit of a few tens of days for the most photoresistant (e.g. adenine, guanine, hypoxanthine). Lifetimes measured in terrestrial orbit are very different from those derived with laboratory experiments. These measurements confirm that it is difficult to simulate the solar spectrum below 200 nm in the laboratory. Results are discussed and highlight the necessity to conduct experiments in orbit, and for longer duration. It also appears that the laboratory measurements made in VUV must be extrapolated very cautiously to the different environments they are supposed to simulate.

© 2010 Elsevier Ltd. All rights reserved.

1. Introduction

The study of the photo stability of organic molecules is an important element in view of the hypothesis that suggests that a significant fraction of organic matter on Earth comes from exogenous deliveries via comets and meteorites. Photochemistry has indeed a leading part in the chemical evolution of organic matter in the Solar System, specifically in the VUV domain (Vacuum Ultra Violet). Therefore experimental studies of the photolysis of organic compounds related to astrophysical environments are common in laboratories, with different kinds of UV sources, monochromatic (e.g. H₂/He (122 nm), Xe (147 nm), CH₄/He (193 nm) (Cottin et al., 2000)) or, polychromatic, simulating a wider range of UV (e.g. H₂ (122 and 160 nm), deuterium discharge lamp (190–400 nm) (Gerakines et al., 1996)). However, it is extremely difficult to simulate the whole range of wavelengths corresponding to the most energetic part of the solar radiation (Cottin et al., 2008) and results measured in the laboratory are difficult to extrapolate to extraterrestrial environments as the spectra of these UV sources are different from the one of the Sun.

Experiments conducted in space, with a direct exposure of samples to the Sun, is a good way to validate ground studies.

In this paper, we focus most particularly on complex organic molecules related to the hypothesis which privileges the import of extraterrestrial organic molecules via comets, meteorites and micrometeorites as the source of terrestrial organic matter. There are many indisputable proofs that several organic compounds such as amino acids and nucleic acid bases (purines & pyrimidines) or their precursors can reach Earth's surface via meteorites (Botta and Bada, 2002; Cronin, 1989; Martins et al., 2007a, 2007b, 2008). The close approach to Earth of comets Hyakutake and Hale-Bopp in 1996 and 1997 respectively, has resulted in the identification of many organic species such as HCN, HNC, CO, CH₃OH, H₂CO, and HNCO (Biver et al., 1999; Bockelee-Morvan et al., 2000; Lis et al., 1997) in addition to other molecules already reported, such as CH₄, C₂H₆ and HCHO (Bockelee-Morvan et al., 2004). The prebiotic relevance of all these organic molecules is widely recognized (Cottin and Despois, 2009). Moreover, the instruments on board of Vega and Giotto space probes (flying-by comet 1 P/Halley) have shown the presence of solid matter in cometary dust in addition to the rather simple volatile compounds detected in the gas phase (Fomenkova, 1999; Kissel et al., 1986). Those results are confirmed by the recent analysis of the organic component of grains collected by the Stardust mission

* Corresponding author. Tel.: +33 1 45 17 15 63; fax: +33 1 45 17 15 64.
E-mail address: cottin@lisa.univ-paris12.fr (H. Cottin).

(Elsila et al., 2009; Sandford et al., 2006) and by laboratory simulations conducted on cometary ice analogs in various laboratories (see for example (Bernstein et al., 1995; Cottin et al., 2001a, 2001b)).

In recent years, several exposure experiments in low Earth orbit (Mir station, FOTON automatic capsules) were conducted in order to study the photostability of organic molecules under direct solar irradiation simulating various astrophysical regions (interplanetary medium, interstellar medium, martian surface). During the exposure on BIOPAN-1 in 1994 and on BIOPAN-2 in 1997 (Barbier et al., 1998, 2002) and Perseus-Exobiologie on the MIR station in 1999 (Boillot et al., 2002), the photodegradation of amino acids was studied, as well as the protective role of meteoritic minerals (such as Montmorillonite) toward organic compounds. On the other hand, (Ehrenfreund et al., 2007) studied the photostability of selected PAHs and fullerene-type molecules in the ORGANICS experiment (BIOPAN-5, flown in 2005). It was concluded that the PAHs are very stable under the space conditions for this experiment, and that longer exposition experiments are needed (on the International Space Station).

In the continuity, a new photochemistry experiment called UVolution has been selected by the European Space Agency (ESA) to be implemented in low Earth orbit (LEO) and in the laboratory. This experiment has been carried out jointly by the Laboratoire Interuniversitaire des Systèmes Atmosphériques (LISA) and the Laboratoire Atmosphères, Milieux, Observations Spatiales (LATMOS). As reference to the space experiments, ground control experiments have been conducted in the laboratory. This paper focuses on cometary and meteoritic related organic material; samples related to organic matter on Mars and Titan also exposed in UVolution are being published separately (see for instance (Stalport et al., in press)). In a first section experimental procedures are presented, then, the rates of photodissociation of the studied molecules are shown in the results section. These data allow us to estimate the half-lives of the molecules in other astrophysical environments (the interstellar medium (ISM) and molecular clouds (IS Cloud)). Both space and laboratory results are compared and discussed.

2. Experimental

2.1. UVolution space experiment setups

UVolution is a small exposition setup dedicated to organic chemistry. It was part of the payload of the BIOPAN 6 space facility, an ESA multi-user space exposure facility, designed by Kayser-Threde, (München, GMBH) for exobiology, radiation biology, radiation dosimetry and material science investigations in space (Demets et al., 2005). BIOPAN6 was set outside of the automated Russian science satellite: FOTON M3 (launched by the Soyuz-U rocket) which orbited the Earth at an altitude of about 300 km. It is a large pan with a deployable lid which is closed and sealed during launch and re-entry operations (more details are presented in Cottin et al. (2008)). Thanks to the UVolution setup, 120 samples could be accommodated for exposure. 60 of these samples are directly exposed to the solar flux while the other 60 samples are not exposed to the solar flux and are used as flight controls (Fig. 1). In the UVolution experiment, for every studied molecule, 2 flight samples were exposed (called flight samples in this paper), 2 others flight samples were not-exposed (called dark controls in this paper) and 2 samples were kept in the laboratory as ground reference (called ground controls in this paper). They were kept in the dark, at room temperature ($\sim 20^\circ\text{C}$) during the period of the flight. With these 3 sets of experiences, the effect of the photochemistry can be studied by subtracting the effect of

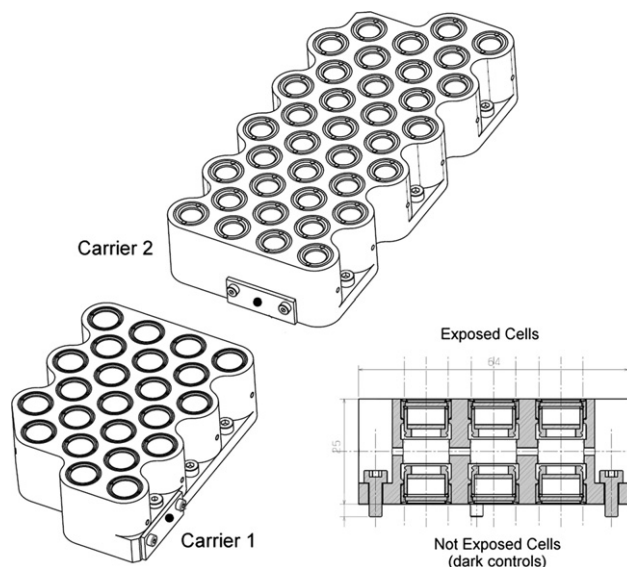


Fig. 1. Accommodation of UVolution flight samples, the two carriers are designed to receive 33 and 27 exposed samples. In each case, both exposed cells and in-flight controls are screwed onto the sample holder (Cottin et al., 2008).

different parameters (including in particular, the effect of solar UV photolysis and the effect of temperature variation).

There is no direct measurement of the solar flux for this experiment. The only data provided was the total amount of solar light received by BIOPAN during the whole mission. It has been evaluated to 29 ± 4.35 solar constant hour in the 220–280 nm range. The exposure flux is derived from an onboard UV-C sensor provided by ESA, the uncertainty of 15% is cross-correlated with orbital calculations provided by RedShift Company (St Niklaas, Belgium). The temperature during the flight oscillated between -22 and $+30^\circ\text{C}$.

2.2. Laboratory experiment setups

Laboratory investigations have been conducted with “classical” laboratory photolysis equipment, in order to compare results obtained in space and in the laboratory. For the sake of clarity, it should be noted that the ground control samples presented in Section 2.1 are actual parts of the space experiment. Laboratory experiments were carried out using other samples, prepared under the same conditions than the space experiment samples.

Samples were photolyzed in the laboratory in a vacuum thermo-controlled reactor connected to a UV lamp. The UV source was a microwave-powered H_2/He -flow lamp (gas mixture: 2% H_2 in He, P inside the lamp = 4 mbar, microwave generator provided by Ophos). Such a lamp delivers an emission spectrum dominated by the Lyman α band (122 nm) in the VUV (Okabe, 1978). The UV flux was measured by N_2O actinometry (Cottin et al., 2000) (more details also in Section 3.2.1). The whole experimental set-up is shown in Fig. 2. Samples are deposited at the bottom of the reactor and are photolyzed through a MgF_2 window as in space. UV photolysis is performed in several time intervals separated by an infrared analysis of the samples, for a total photolysis time of 4–15 h depending on the molecule.

2.3. Sample preparation

2.3.1. Targeted compounds

This paper focuses on results obtained for compounds related to meteorites and comets, of astrobiological significance. Glycine and four purine molecules (adenine, guanine, xanthine and

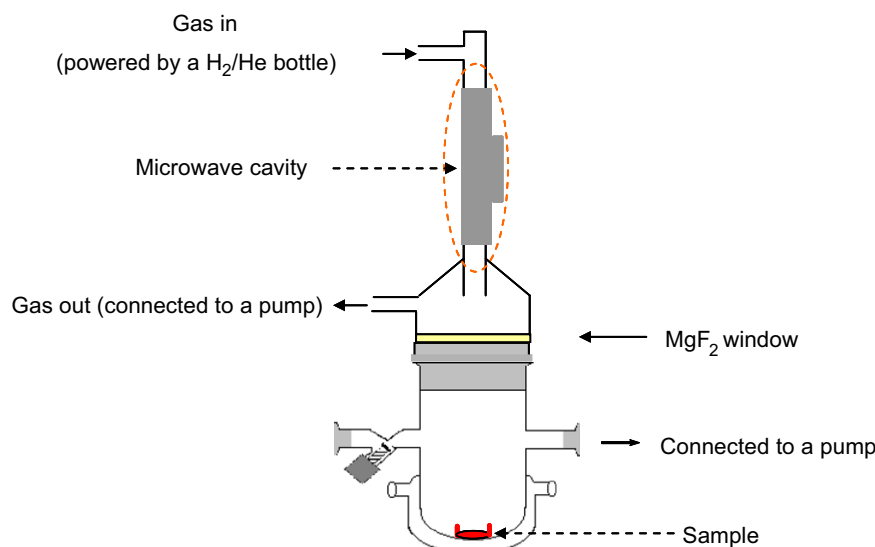


Fig. 2. A schematic drawing of a H₂/He flow lamp. The lamp is fed continuously by a H₂/He bottle and is connected to a vacuum pump. Samples are put at the bottom of the reactor to be photolyzed.

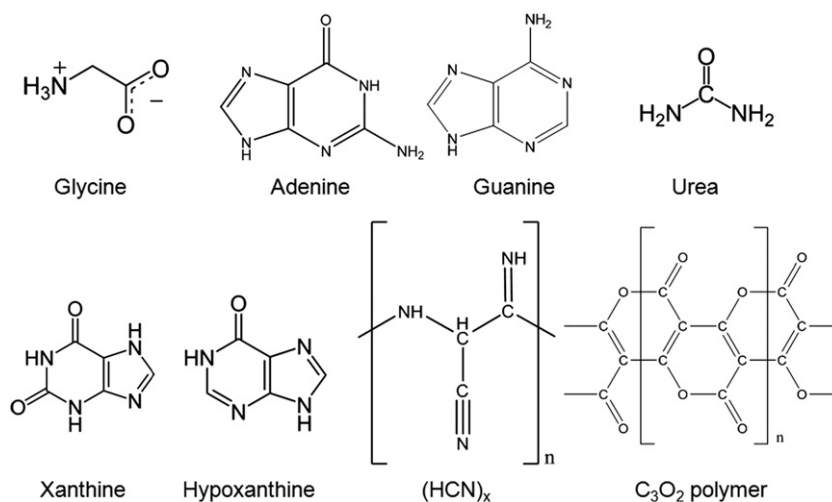


Fig. 3. Chemical formulae of the 8 molecules discussed in this paper. The HCN polymer is a complex macromolecular compound containing double or triple CN bonds, the formula represented in this figure is one of the possible structures. The structure of C₃O₂ polymer is suggested by Gunne et al. (2005).

hypoxanthine) have been selected because they have been detected in carbonaceous meteorites (especially in Murchison meteorite) (Botta and Bada, 2002; Hayatsu, 1964; Hayatsu et al., 1975; van der Velden and Schwartz, 1977; Martins et al., 2008). Xanthine and hypoxanthine can be obtained from the two nucleobases guanine or adenine through a deamination reaction. Purine compounds have also been tentatively detected by mass spectrometry in comet 1P/Halley (Kissel and Krueger, 1987). Laboratory simulations on interstellar and cometary ice analogs have demonstrated that glycine (among other amino acids), could also be present in comets (Bernstein et al., 2002). HCN and C₃O₂ polymers can be synthesized after processing by photons and protons of ices containing HCN (Gerakines et al., 2004) and CO (Gerakines and Moore, 2001) and are suspected as the origin of distributed sources of CN and CO, respectively, when they are heated and/or photolysed by the Sun (Cottin and Fray, 2008). Urea has also been selected because laboratory experiments have demonstrated that it can be synthesized in interstellar and cometary ices (Agarwal et al., 1985; Raunier et al., 2004). Chemical formulae of all the molecules in this study are grouped in Fig. 3.

All molecules were purchased from Sigma-Aldrich (purity > 99%) except for (C₃O₂)_n and HCN polymer which have been kindly provided by Pr. Johannes Beck (Institut für Anorganische Chemie der Universität Bonn), and Pr. Robert Minard (Penn State Astrobiology Research Center and Department of Chemistry, Penn State University), respectively.

2.3.2. Exposure cells

Two kinds of exposure cells were used for the UVolution experiment: open and closed ones (Fig. 4). The open cells are made of a cylindrical aluminium body and a MgF₂ window (thickness: 1 mm, diameter: 9 mm). The closed cells are made of two cylindrical aluminium bodies which can be screwed one into the other; two windows in MgF₂ are glued on both sides of cell (for more details about the cells, see Cottin et al. (2008)). MgF₂ windows transmit UV photons down to 120 nm allowing the photolysis of the samples deposited on the inner side of the window. But in the open cells, the volatile fragments resulting from photolytic processes are released into vacuum (laboratory setup or space) and lost for analysis. Closed cells can be used for

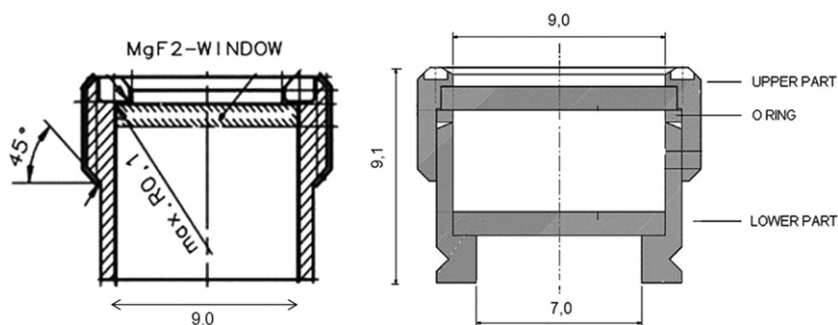


Fig. 4. At left: open cells (height: 9.1 ± 0.1 mm, Φ : 9 ± 0.1 mm) and at right: close cells (height: 9.1 mm, Φ : 9 mm).

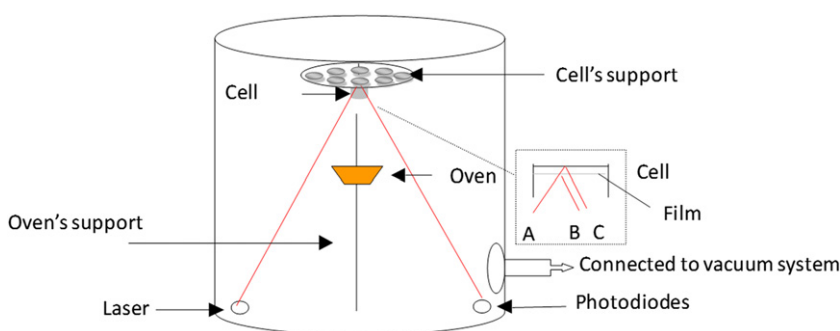


Fig. 5. Schematic drawing of the sublimation reactor, at one side of the bottom of the reactor, a laser emits a monochrome light (580 nm) which is reflected by the film and the cell's window. A photodiode is installed at the other side; it receives the reflected light and measures variations in intensity related to the thickness of the films.

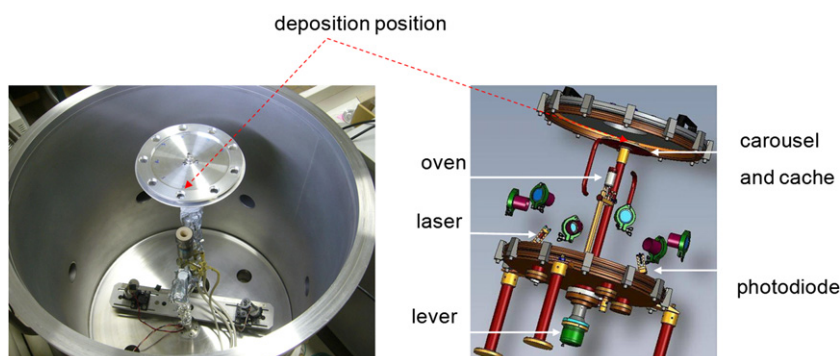


Fig. 6. At the right, upside view of the reactor, the 9 positions sample holder (carousel) allows a series of 8 films (with 1 blank position), the carousel is protected by a metal cover that has only one opening just in front of the oven (above). At the left, the different components are shown on a 3D drawing of the reactor.

gas mixture samples, or to analyse the gaseous products resulting from the photolytic processes. Most of the compounds related to comets and meteorites were exposed in open cells, only C_3O_2 polymer samples were accommodated in closed cells.

2.3.3. Deposition method by sublimation and re-condensation

Most of our samples were prepared in a vacuum sublimation system. Inspired by the work of the team from the Leiden Observatory in the Netherlands (ten Kate et al., 2005), we have developed a sublimation reactor (Figs. 5 and 6) (built by Meca 2000 company (France)) in which homogenous organic films with a controlled thickness can be deposited on the windows of our exposition cells. The sublimation reactor is connected to a secondary vacuum system. At the beginning of the deposition procedure the vacuum in the reactor is about 10^{-4} mbar. Then, the desired molecule is deposited as a powder in an oven and its

temperature is set so that the molecule would slowly sublime and re-condense homogeneously on the window of the cell placed in front of the oven. During the deposition, the pressure is maintained at about 10^{-4} mbar in the reactor. Our device is conceived so that up to 8 cells can be prepared without breaking the vacuum in the reactor (see Fig. 6).

When a deposition process starts, one of the positions that can be called the "deposition position" is just in front of the oven. The sublimated molecules condense directly on the cell placed on the "deposition position" while the cells placed in other positions are "protected" by a metal cover that has just one opening at the "deposition position" (i.e. in front of the oven). We can rotate the carousel to move the other cells on the "deposition position", using a lever located at the bottom of the reactor (outside).

The thickness of the films is controlled by interferometry. The laser beam undergoes multiple reflexions inside the organic layer. The reflected beams are superimposed and create interferences

which can be either constructive or destructive. As the thickness of the film increases, the intensity on the photodiode changes periodically. Each period (2π) corresponds to an “equal thickness” (Fig. 7) that can be calculated by $\Delta e = \lambda/2n\cos i$ (1), where λ is the wavelength of the incident light, n the refractive index of organic matter, and i the incident angle.

The thickness of the film is proportional to the number of periods and is determined to be thin enough to allow (i) a quantitative analysis by transmission infrared spectroscopy (optically thin in the infrared), (ii) the observation of a first order decay during preliminary laboratory photolysis experiments (optically thin in the VUV), and (iii) thick enough to have sufficient sample in the cell even after its return to Earth for quantitative analyses by transmission infrared spectroscopy.

In order that all molecules of a sample are homogeneously photolyzed, our films are expected to be uniform (at surface and in depth). A differential interference contrast microscope (Veeco Wyko NT 1100) is used for the calibration of the thickness of films and for the control of their homogeneity. After the preparation of a sample used for thickness calibration, characterized by a number of interference fringes, a portion of the organic film is removed along a diagonal of the sample by digging a furrow with a hard tip. The level difference between the film and its support (window) can be measured with an interference microscope. A typical image is shown in Fig. 8. The interference microscope can scan a zone of $1.2 \text{ mm} \times 0.9 \text{ mm}$ and the in-depth probe measures the thickness of films. The results show a good homogeneity of

our films. The surface of the film is fairly smooth. Typically, the thicknesses of the samples are some hundreds nanometers (one interference fringe $\sim 300 \text{ nm}$).

2.3.4. Deposition method by solvent evaporation

HCN or C_3O_2 polymers are pyrolyzed and altered rather than being sublimated, when heated. We have used an evaporative method to prepare films of these two molecules. This involves: first dispersing by mechanical agitation the compound as powder throughout a solvent ($\text{H}_2\text{O}/\text{CH}_3\text{COCH}_3$: 3/5) to prepare a suspension, and then deposit this solution in the cell. Finally, the sample is obtained after the total evaporation (vacuum evaporation) of the solvent. This method was used by Boillot et al. (2002). The principal defect of this method is that the films are not homogenous and we cannot control their thickness.

2.4. Analysis method (FTIR)

A Fourier Transform Infrared (FTIR) spectrometer (Perkin Elmer—BXII) is used as main analytical tool. Spectra are acquired by transmission through the MgF_2 windows, with a resolution of 4 cm^{-1} and between 4000 and 1000 cm^{-1} . Indeed MgF_2 is not transparent for lower wavenumbers (MgF_2 cut-off in the infrared domain is at 1000 cm^{-1} ($10 \mu\text{m}$)). Infrared spectra are measured in the laboratory before and after the experiment. The spectra of the samples are compared to reference spectra to search for new compounds. Relative quantification is achieved by measurement of the area of a characteristic absorption feature of the studied molecule. No absolute measurement is required in the case of the first order kinetics we are dealing with. This allows quantitative analysis of the samples through both open and closed cells.

2.5. Methods of determination of photolysis reaction constants

The goal in this study is to measure the photodestruction rates of the targeted compounds, expressed as photodestruction constants J (in s^{-1}). The photo-destruction reaction of a molecule

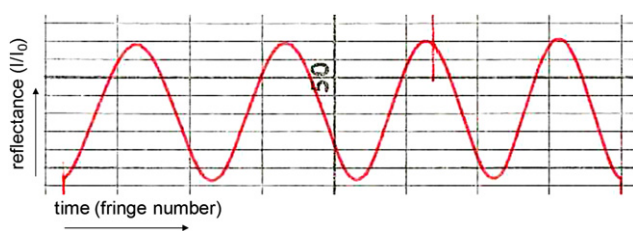


Fig. 7. A measurement recorded by the photodiode which corresponds to a film of 4 times “equal thickness”.

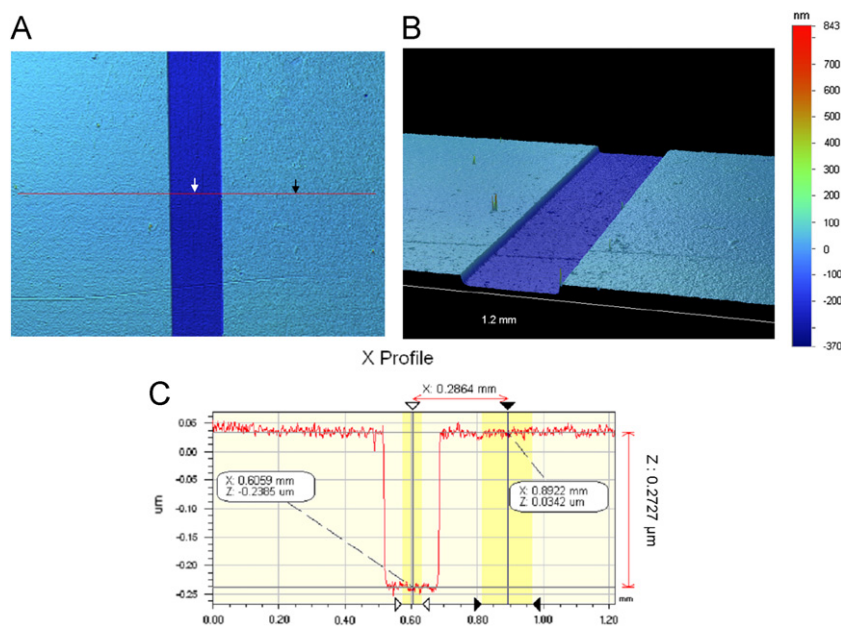


Fig. 8. Example of a measurement of thickness with interference microscopy. (A) Upside view ($0.92 \text{ mm} \times 1.2 \text{ mm}$) of an organic film, the clear part is the top level of film, the dark part corresponds to the trench performed using a hard tip. (B) 3-dimensional image. (C) Measurement of thickness, the vertical profile representing the height (thickness) of the film along the axis represented in red on the upside image, the thickness measured is $0.273 \mu\text{m}$.

can be determined as

$$N \xrightarrow{h\nu} \text{products} \quad (2)$$

If the sample is optically thin, the decrease of the molecule's number (N_t) follows a first order kinetic (Eq. (3)). This hypothesis was validated with laboratory experiments (Section 3.2):

$$\frac{d[N]}{dt} = -J[N] \quad (3)$$

The integration of Eq. (3) leads to

$$\ln(N_t/N_0) = -Jt \quad (4)$$

where J is the photodestruction constant reflecting the kinetics of the reaction. By definition: $J = \int \sigma_\lambda^{abs} \phi_\lambda I_\lambda d\lambda$, I_λ is the photons flux (photon $\text{cm}^{-2} \text{s}^{-1}$), σ_λ^{abs} the absorption cross section (cm^2), and ϕ_λ the quantum yield of photodissociation. The last two parameters depend also on λ . It should be noted that there is only little data on these two parameters in the literature. However the constant J can be determined experimentally.

Assuming that the number of molecules is proportional to the area of infrared bands, J is calculated with Eq. (3) using a plot of the logarithm of the relative abundance of the studied compound as a function of time.

3. Results

The results of infrared analyses are processed with the same method as for the space experiment and for the laboratory simulations. Results are presented separately and will be compared. These comparisons allow us to discuss the validity of the measurements of kinetics of photolysis of organic molecules submitted to solar UV, and their extrapolation to astronomical environments.

3.1. Space experiment

3.1.1. Glycine

The case of glycine is explained as an illustration of the procedure conducted on the various samples. The IR spectrum of a film of glycine is shown in Fig. 9. The assignments of the infrared peaks have been performed thanks to the studies of Rosado et al. (1998) and Uvdal et al. (1990) and are described in Table 1. We observe the presence of bands due to NH_3^+ groups as well as the absence of the characteristics of bands of O–H stretching which should be located around 3600 cm^{-1} (Rosado et al., 1998). This

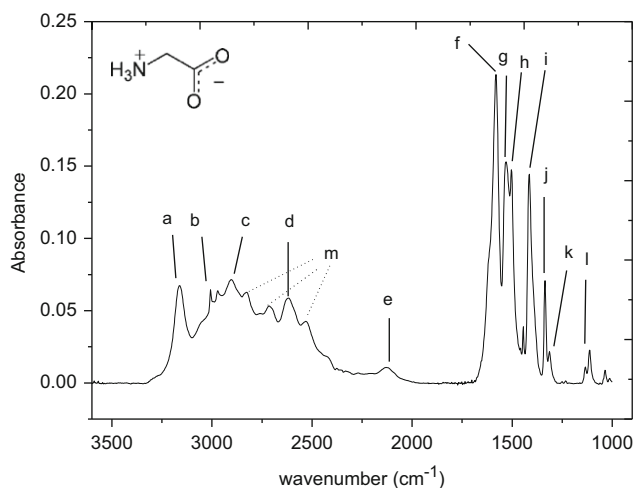


Fig. 9. IR spectrum of solid glycine in the range $4000\text{--}1000 \text{ cm}^{-1}$.

Table 1

Spectral assignments for the glycine films on a MgF_2 window. ν : stretching; δ : bending; ω : wagging; ρ : rocking; tw : twisting; τ : torsion; s : symmetric; as : asymmetric (Rosado et al., 1998; Uvdal et al., 1990).

Label	Wave number (cm^{-1})	Band assignment
a	3163	$\nu_{as}\text{NH}_3^+$
b	3007	$\nu_{as}\text{CH}_2$
c	2899	$\nu_s\text{NH}_3^+$
d	2619	$\nu_{as}\text{NH}_3^+ + \nu\text{CN}$
e	2123	$\nu_{as}\text{NH}_3^+ + \tau\text{NH}_3^+$
f	1581	$\nu_{as}\text{COO}^-$
g	1530	$\delta_{as}\text{NH}_3^+$
h	1503	$\delta_{as}\text{NH}_3^+$
i	1414	ωCOO^-
j	1335	ωCH_2
k	1313	twCH_2
l	1113	ρNH_3^+
m	2830, 2719, 2528	Band combinations ^a

^a The bands at 2830 , 2719 and 2528 cm^{-1} are related to Fermi resonance with band combinations. These assignments show that the glycine is in zwitterionic form ($^+\text{NH}_3\text{CH}_2\text{COO}^-$).

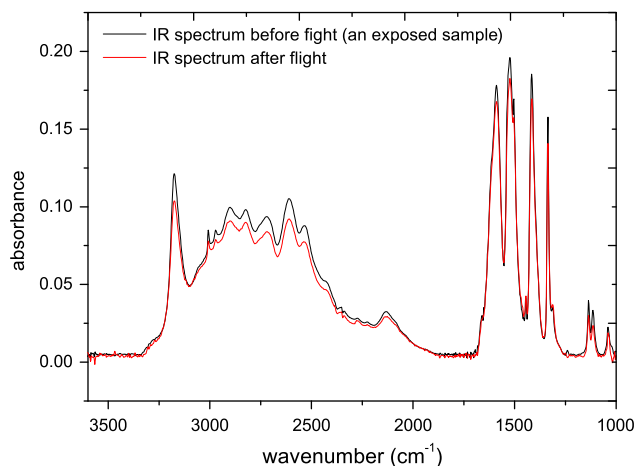


Fig. 10. Comparison of IR spectra before and after flight of an exposed flight sample. Decreases in intensity are visible in all intense bands ($3000\text{--}1000 \text{ cm}^{-1}$).

spectrum is characteristic of the zwitterionic form of the glycine ($^+\text{NH}_3\text{CH}_2\text{COO}^-$) which is formed by an internal transfer of proton from the $-\text{COOH}$ to the $-\text{NH}_2$ group.

Fig. 9 shows two main features in the infrared spectra: a series of overlapping bands extending from 3300 to 2000 cm^{-1} , corresponding mainly to the NH vibration, but also vibrations of CH or CN, and another region of intense bands around 1500 cm^{-1} , which are spectral signatures of COO^- , C–H and NH_3^+ . Thus all samples of glycine were characterized with IR spectroscopy. They are all in the zwitterionic form. However, the IR spectra appear to be slightly different from one sample to another in terms of spectral intensity (Figs. 10–12). These spectral differences result of different crystalline forms of glycine film. Indeed solid glycine can exist in three crystalline forms α , β , and γ (Albrecht and Corey, 1939). Transformations between α glycine, β glycine (metastable) and γ glycine are well studied. The α to γ transition occurs at high humidity (Iitaka, 1960), while the opposite processes can occur on heating to around $170 \text{ }^\circ\text{C}$ (Sakai et al., 1992). The β form can be formed from gas phase via sublimation processes of α or γ glycine in vacuum. But it transforms rapidly to α or γ form in the presence of moisture at room temperature (Liu et al., 2008).

The samples in our experiment are a mixture of α and γ form. Differences between samples are probably due to humidity and to

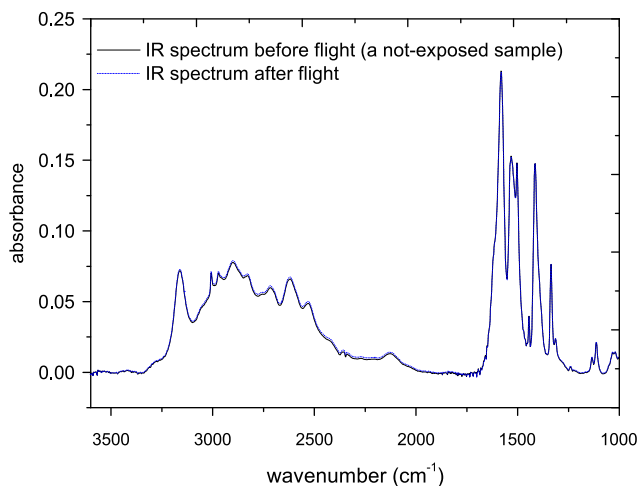


Fig. 11. Comparison of IR spectra before and after flight of a dark control sample. No significant changes between the two spectra (3000–1000 cm⁻¹).

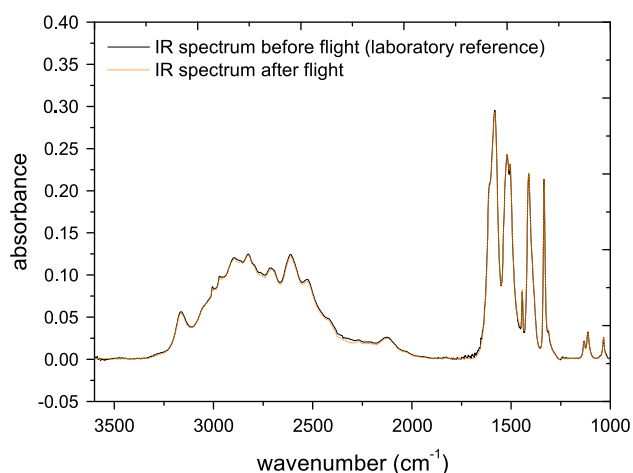


Fig. 12. Comparison of IR spectra before and after flight of a ground control sample. No significant changes between the two spectra (3000–1000 cm⁻¹).

the heating duration during the deposition, but we have not been able to strictly control this parameter in due time before the samples had to be handed over for integration before the launch. Once the samples are ready and analyzed for the first time by infrared spectroscopy, no change in the spectral shape is shown over very long period of times (for flight samples, dark and ground controls), which means that such transformations occur during the deposition process itself, or in the very few minutes after the samples are at atmospheric pressure after their preparation. The different crystalline forms of our samples do not seem to affect the results within error bars as it will be shown later.

Figs. 10–12 show the comparison of the infrared spectra before and after flight for three glycine's cells (exposed flight cell, not exposed flight cell, and ground control reference cell). For the exposed cell, the shape spectra of the film before and after photolysis are identical. A decay of the band intensity is obvious, but no new bands are appearing. No difference can be observed for the others samples. It suggests that all the products of photolysis of glycine are gaseous and that they have escaped in space. Barbier et al. (2002) show that no polymerisation occurred in the glycine samples during Biopan II experiment. This result is also coherent with the one presented in Ehrenfreund et al. (2001) where the production of CO₂ and HCN during the UV irradiation of glycine in Ar matrix is reported. Moreover, the crystallisation state seems not to be affected by the UV irradiation.

The results show that the decrease of band intensities is only due to decomposition of glycine. Two spectral domains (between 3400 and 1900 cm⁻¹ and between 1700 and 1200 cm⁻¹) were integrated to calculate the amount of molecules before and after the UV exposition. The results for the bands integrations are shown in Table 2. For the 2 exposed cells, a decrease of about 10 percent is observed for all band intensities, whereas no significant variation is observed for the dark control samples. Table 2 shows that for each category of samples, the rate of photo-destruction is consistent between them; only the flight exposed cells show a significant decay due to photolysis. The two infrared patterns show a similar rate of photo-destruction. Ehrenfreund et al. (2001) suggest that the photodestruction mechanism of glycine starts with the separation of the carboxyl group:

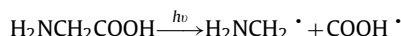


Table 2

Results of the bands integration of the glycine's spectra. Uncertainty on the area measurement with our experimental setup is about 2%.

Cell no.	Description	Area band 1 (cm ⁻¹) (around 3000 cm ⁻¹) before/after	Variation (%)	Area band 2 (cm ⁻¹) (around 1500 cm ⁻¹) before/after	Variation (%)
GLY_01	Exposed	44.8/40.0	-11	33/29.8	-10
GLY_02	Exposed	33.6/30.5	-9	24.3/21.6	-11
GLY_03	Not exposed	41.8/41.9	0	26/25.6	-2
GLY_04	Not exposed	38/37.7	-1	23.9/23.9	0
GLY_05	REF, lab	75.4/74.6	-1	42.0/42.0	0
GLY_06	REF, lab	50.0/50.0	0	22.9/23.1	0

Table 3

Interpretation of 8 data from two IR measurements of both exposed flight samples of glycine, these data allow a to draw linear regression (Fig. 11).

Analyzed Band	Time (s): before the flight, noted 1 s; after the flight, noted 104,400 s (29 h × 3600 s/h)	[N] _t /[N] ₀	ln([N] _t /[N] ₀)
Samp_1 (3400–1900 cm ⁻¹)	1 (before the flight)	1	0
Samp_1 (1700–1200 cm ⁻¹)	1 (before the flight)	1	0
Samp_2 (3400–1900 cm ⁻¹)	1 (before the flight)	1	0
Samp_2 (1700–1200 cm ⁻¹)	1 (before the flight)	1	0
Samp_1 (3400–1900 cm ⁻¹)	104,400 (after the flight)	0.892	-0.114
Samp_1 (1700–1200 cm ⁻¹)	104,400 (after the flight)	0.908	-0.097
Samp_2 (3400–1900 cm ⁻¹)	104,400 (after the flight)	0.899	-0.106
Samp_2 (1700–1200 cm ⁻¹)	104,400 (after the flight)	0.890	-0.117

With the rearrangement of the proton in the COOH^{\cdot} and $\text{H}_2\text{NCH}_2^{\cdot}$ radicals, CO_2 and methylamine (CH_3NH_2) would be formed. This can lead to the formation of HCN. All those products are gaseous.

A first order kinetics being assumed, J is calculated from Eq. (3). For each sample, only two IR measurements, before and after the flight, are possible. Nevertheless, we have studied two samples and for each one, two IR domains have been considered. A linear regression through these 8 points (Table 3) allows us to determine the photodissociation rate which is equal to the slope of the logarithm of the relative amount of molecules as a function of time (see Fig. 13).

$J = -\text{slope} \pm t_{(n-2)}\sigma(1+1/n)^{1/2}$, with measurement number $n=8$, $t=2.45$ from a Student's t -distribution (confidence interval 95% and degree of liberty $(n-2)=6$). Finally, we calculate that the photodestruction rate of glycine is equal to $1.0 \pm 0.1 \times 10^{-6} \text{ s}^{-1}$.

3.1.2. Purine molecules (xanthine, hypoxanthine, adenine and guanine)

As for the glycine samples, the results of infrared analysis of the 4 purine molecules studied are presented in this section, with a first step in identifying the IR spectral bands. Then the results of quantitative analysis are presented, which allow us to calculate the photodestruction rates of these four molecules.

The IR spectra of xanthine, hypoxanthine, adenine and guanine films taken before the flight are show in Figs. 14–17, respectively.

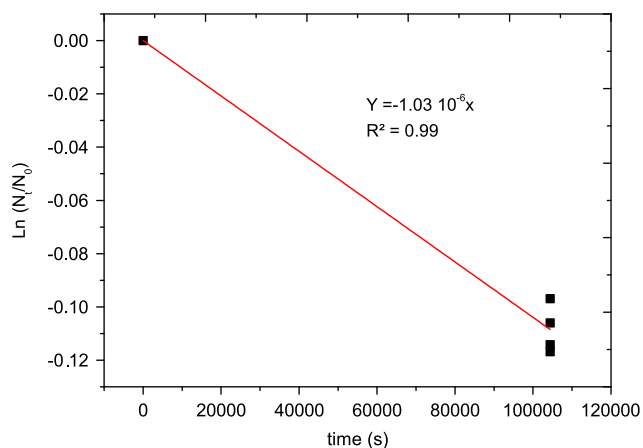


Fig. 13. Photodestruction translated by temporal evolution of the amount of glycine, the Y-axis is the logarithm of the abundance of glycine, N_0 : initial abundance, N_t : abundance final.

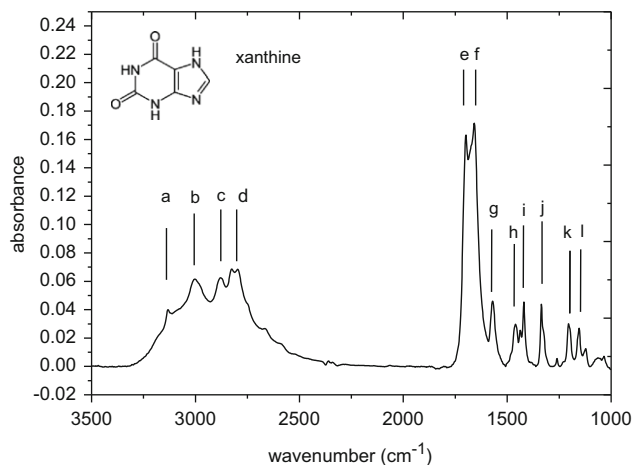


Fig. 14. IR spectrum of a film of xanthine in the region $(3500\text{--}1000 \text{ cm}^{-1})$.

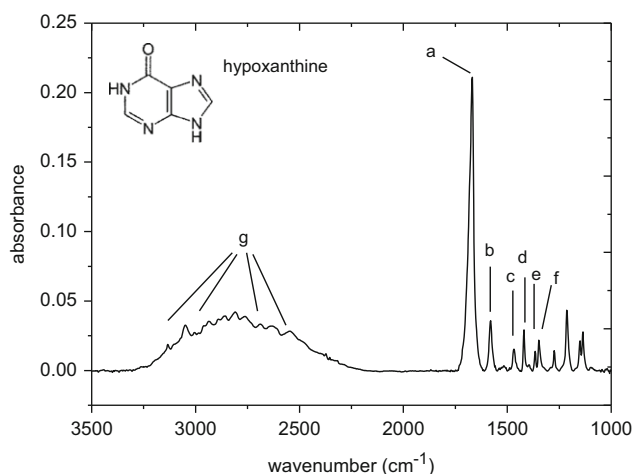


Fig. 15. IR spectrum of a film of hypoxanthine in the region $(3500\text{--}1000 \text{ cm}^{-1})$.

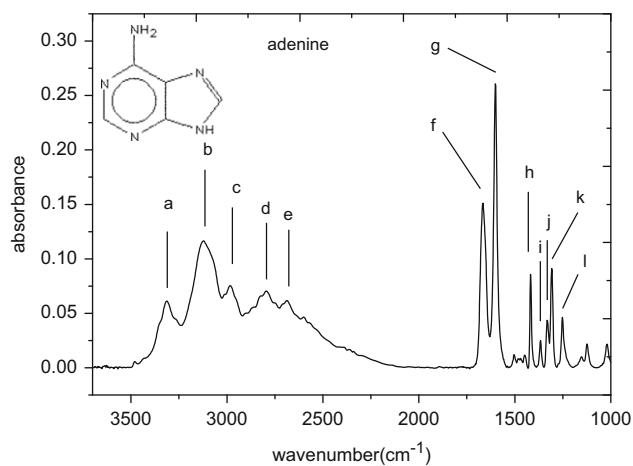


Fig. 16. IR spectrum of solid adenine in the range $4000\text{--}1100 \text{ cm}^{-1}$.

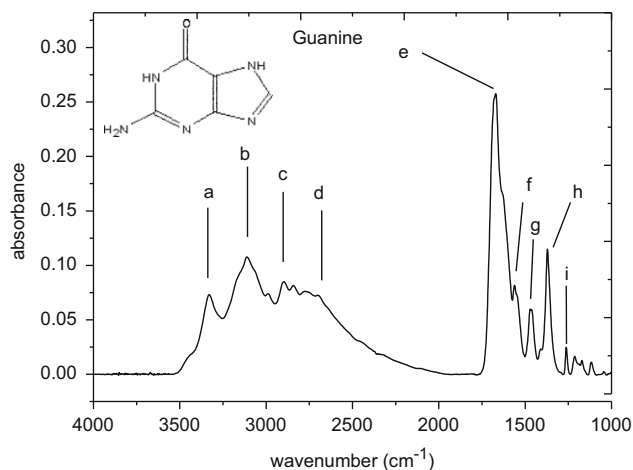


Fig. 17. IR spectrum of solid guanine in the range $4000\text{--}1000 \text{ cm}^{-1}$.

The band assignments for these 4 compounds have been performed thanks to the studies of (Delabar and Majoube, 1978; Gunasekaran et al., 2005; Hiraikawa et al., 1985; Mathlouthi et al., 1984) (Fernandez-Quejo et al., 2005) and are presented in Tables 4–7.

Table 4

Assignment of IR bands of xanthine (sediment deposition), ν stretching; δ , bending; s, symmetrical; as, asymmetric (Gunasekaran et al., 2005).

Label	Wave number (cm^{-1})	assignments
a	3132	νNH
b	3003	$\nu_{\text{as}}\text{NH}$
c	2878	$\nu_{\text{s}}\text{NH}$
d	2826, 2796	νCH
e	1698	νCN
f	1658	$\nu_{\text{as}}\text{C}=\text{O}$
g	1569	$\nu_{\text{s}}\text{C}=\text{O}$
h	1460	δCH
i	1420	$\nu_{\text{s}}\text{C}=\text{O}$
j	1335	νCN
k	1205	$\nu_{\text{as}}\text{CN}$
l	1154	$\nu_{\text{as}}\text{CN}$

Table 5

Assignment of IR bands of hypoxanthine (solid film), ν stretching, δ , bending; (Fernandez-Quejo, 2005). The broad band between 3300 and 2100 cm^{-1} corresponds to different vibration modes attributed to NH and CH bonds. No measurements are referenced for the bands of this region; however, theoretical data are published in the same reference.

Label	Wavenumber (cm^{-1})	Assignments
a	1669	$\nu\text{C}=\text{O}$
b	1580	νCN , δCH
c	1468	δCH
d	1420	δCH , νCN
e	1365	δCH
f	1347	δCH
g	3300–2100	Different modes of vibration of NH and CH bonds

Table 6

Spectra assignments for adenine film on a MgF_2 window, ν stretching; δ , bending (Hirakawa et al., 1985; Mathlouthi et al., 1984).

Label	Wave number (cm^{-1})	Band assignment
a	3314	$\nu_{\text{s}}\text{NH}_2$
b	3122	$\nu_{\text{as}}\text{NH}_2$
c	2984	νNH
d	2798	νCH
e	2689	νCH
f	1665	δNH_2
g	1600	νCN
h	1417	$\delta\text{N}=\text{C}-\text{H}$
i	1366	δCH
j	1330	νCN
k	1307	νCN
l	1251	δNH

Table 7

Spectra assignments for guanine film on a MgF_2 window, ν stretching; δ , bending (Delabar and Majoube, 1978; Mathlouthi et al., 1984).

Label	Wave number (cm^{-1})	Band assignment
a	3330	$\nu_{\text{a}}\text{NH}_2$
b	3113	$\nu_{\text{s}}\text{NH}_2$
c	2898	νNH
d	2699	νCH
e	1674	νCO , δNH_2
f	1563	$\nu\text{C}=\text{N}$
g	1467	$\nu\text{C}-\text{N}-\text{H}$
h	1372	δNH
i	1263	νCN

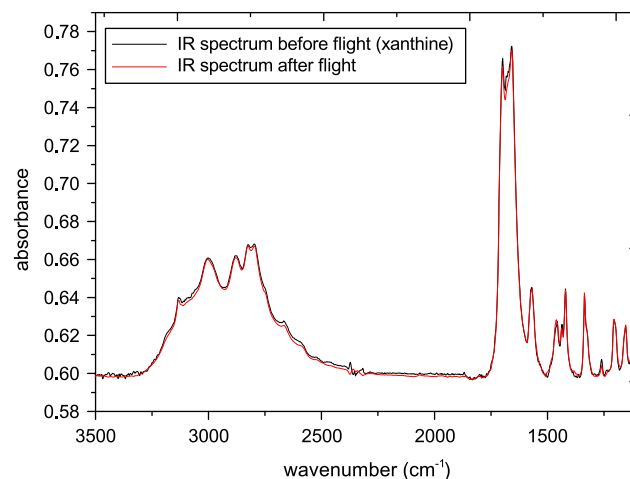


Fig. 18. Comparison of two spectra before and after the flight of an exposed flight sample of xanthine.

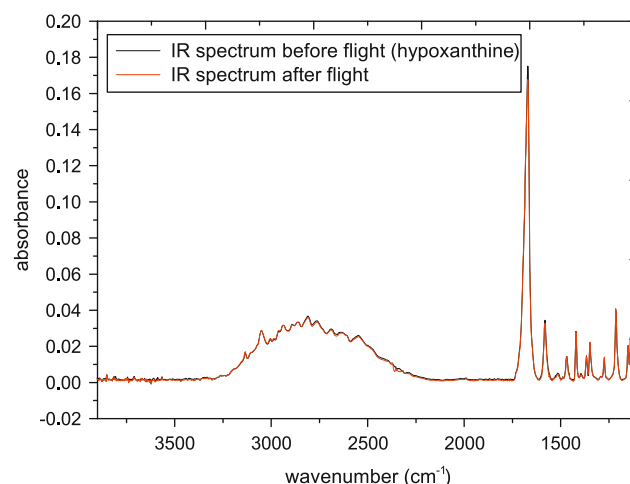


Fig. 19. Comparison of two spectra before and after the flight of an exposed flight sample of hypoxanthine.

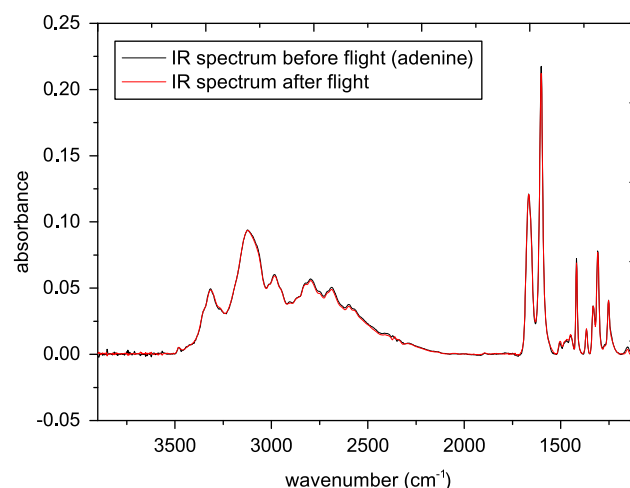


Fig. 20. Comparison of two spectra before and after the flight of an exposed flight sample of adenine.

The assignments of IR bands characteristics of the four purine molecules confirm that the heating during the process of sublimation does not alter the nature of these compounds.

The comparison of these spectra with those after the flight allows us to evaluate the effects of solar UV photolysis. As for glycine, the spectra before and after the flight of each molecule are stacked in Figs. 18–21 for xanthine, hypoxanthine, adenine and guanine, respectively.

No new band appears in any spectra after the flight. This suggests that there would be no new species formed in solid phase during the photolysis of the four purines. Except xanthine whose post-flight spectrum is slightly different than the pre-flight (a small decrease in intensity of the bands) (Fig. 18). The post-flight spectra of the other three molecules are not changed compared to spectra of respective pre-flight (the spectra are virtually superimposed). This shows that these purines are relatively resistant towards solar UV. The results of quantitative analysis on the range of spectral bands are presented in Table 8. It is noteworthy that the spectra presented in Figs. 18–21 are those of samples exposed in flight, the spectra of dark and

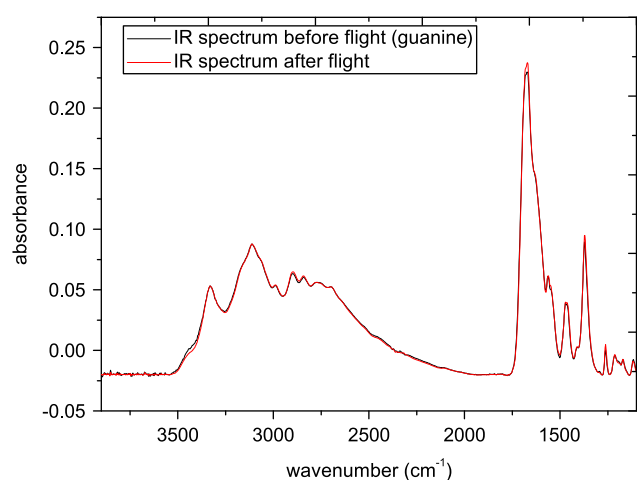


Fig. 21. Comparison of two spectra before and after the flight of an exposed flight sample of guanine.

Table 8
Results of IR spectral bands integrations for the four purines molecules, the three categories (exposed cells, unexposed cells and reference laboratories) are presented.

Nature and cells' no.	Description	Area band1 (cm ⁻¹) (around 3000 cm ⁻¹) before/after	Variation (%)	Area band 2 (cm ⁻¹) (around 1500 cm ⁻¹) before/after	Variation (%)
Xanthine_01	Exposed	30.3/28.5	-6	16.0/15.2	-5
Xanthine_02	Exposed	32.3/30.6	-5	15.3/14.7	-4
Xanthine_03	Not exposed	31.0/31.2	0	15.8/15.8	0
Xanthine_04	Not exposed	36.9/36.7	0	19.0/19.0	0
Xanthine_05	REF, lab	24.9/24.9	0	16.7/16.6	-1
Xanthine_06	REF, lab	23.6/23.7	0	11.7/11.8	1
Hypoxanthine_01	Exposed	20.2/20.1	0	7.32/7.31	0
Hypoxanthine_02	Exposed	20.8/20.9	0	6.97/6.95	0
Hypoxanthine_03	Not exposed	23.2/23.2	0	8.28/8.29	0
Hypoxanthine_04	Not exposed	23.7/23.7	0	7.36/7.38	0
Hypoxanthine_05	REF, lab	20.3/20.4	0.6	6.01/5.98	-0.5
Hypoxanthine_06	REF, lab	23.7/23.7	0	6.65/6.63	0
Adenine_01	Exposed	47.1/46.9	0	8.84/8.74	-1
Adenine_02	Exposed	57.1/56.3	-1	10.8/10.6	-2
Adenine_03	Not exposed	45.4/45.3	0	9.27/9.22	0
Adenine_04	Not exposed	47.8/47.0	1.6	10.1/9.97	-1
Adenine_05	REF, lab	41.8/41.2	-1	8.59/8.54	-1
Adenine_06	REF, lab	33.5/33.2	0	6.94/6.92	0
Guanine_01	Exposed	38.9/38.9	0	16.9/17.0	0
Guanine_02	Exposed	77.4/77.7	0	35.6/35.6	0
Guanine_03	Not exposed	53.8/53.6	0	25.1/25.1	0
Guanine_04	Not exposed	47.0/46.4	-1	19.0/19.1	0
Guanine_05	REF, lab	31.1/31.1	0	14.9/15.2	1
Guanine_06	REF, lab	70.0/69.8	0	35.3/35.3	0

ground control samples show no spectral change for these four molecules.

The results show that the variation in term of IR bands area for xanthine is about 5%, but no change is measurable for the other three molecules. Using the same method than for glycine, a linear regression allows us to calculate the constant J photodestruction of xanthine (Fig. 22). The slope is equal to J , we deduce that $J = 5 \pm 1 \times 10^{-7} \text{ s}^{-1}$. The purines are more resistant to solar UV than glycine, which is coherent with the results presented in Schwel et al. (2006) where ionization energies were measured to be higher for the nitrogenous bases (adenine and purine, etc.) than for amino acids.

3.1.3. Urea

With the same analytical procedures as those described above, the results for urea are presented in this section. First, we present the assignment of IR spectral bands (Fig. 23) in Table 9 using Kutzelnigg et al. (1961) and Rousseau et al. (1999). Then the quantitative analysis of the results is shown in Table 10.

The IR spectra before and after the flight of urea are presented in Fig. 23. No new spectral features can be observed in the spectrum of post-flight analysis, the two spectra are indeed stackable. The quantitative results (Table 10) show that exposed flight samples present no significant change in the region (4000–1000 cm⁻¹). The other samples give similar results. Note that in Fig. 23, the IR bands of urea appears to be saturated (absorbance values > 3). Indeed, urea sublimates at relatively low temperature (90 °C) suddenly and rapidly under our experimental conditions. We were unable to control its deposition inside the cells. Our films are too thick to quantify its photolysis.

3.1.4. Carbon suboxide polymer (C₃O₂)_n

The carbon suboxide polymer (C₃O₂)_n is a red-brown amorphous solid, strongly hygroscopic. The samples were prepared by evaporation method in a glove box (under 1.2 bar nitrogen) to avoid contact with water vapour.

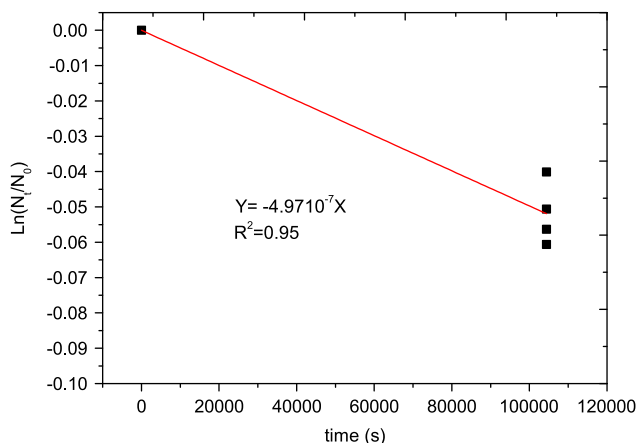


Fig. 22. Photodestruction of xanthine: the evolution of the amount of matter as a function of time. The Y-axis is the logarithm of the abundance of xanthine, N_0 : initial abundance, N_t : final abundance.

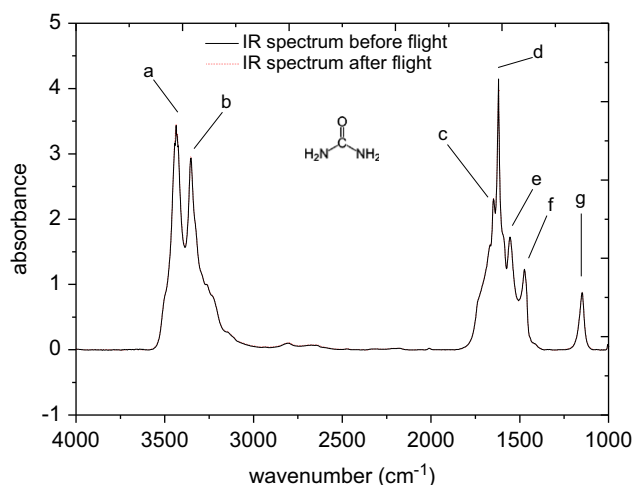


Fig. 23. IR spectrum of a solid urea sample in the range 4000–1000 cm^{-1} , two spectra (before and after the flight) are superimposed on this figure.

Table 9
Spectra assignments for urea film on a MgF_2 window, ν stretching; δ , bending; ρ rocking (Kutzelnigg et al., 1961; Rousseau et al., 1999).

Label	Wave number (cm^{-1})	Band assignment
a	3437	$\nu_a\text{NH}_2$
b	3351	$\nu_s\text{NH}_2$
c	1647	$\delta_s\text{NH}_2$
d	1620	δNH_2
e	1554	νCO
f	1473	$\nu_a\text{C-N}$
g	1149	$\rho_s\text{NH}_2$

Table 10
IR analysis results of urea for both exposed cells, not-exposed cells and ground reference cells.

Cell no. nature	Description	Area band 1 (cm^{-1}) (around 3000 cm^{-1}) before/after	Variation (%)	Area band 2 (cm^{-1}) (around 1500 cm^{-1}) before/after	Variation (%)
UREA_01	Exposed	589/582	-1	443/444	0
UREA_02	Exposed	640/666	4	452/451	0
UREA_03	Not exposed	571/578	0	412/429	4
UREA_04	Not exposed	633/642	0	392/388	-2
UREA_05	REF, lab	553/563	2	417/413	-1
UREA_06	REF, lab	547/563	3	377/380	0

The IR spectrum of $(\text{C}_3\text{O}_2)_n$ is shown in Fig. 24, the most intense bands are between 1820 and 1300 cm^{-1} . The assignments of $(\text{C}_3\text{O}_2)_n$ are more difficult compared to other studied molecules, because there are no references converging to the same interpretation of these spectra in the literature (Blake et al., 1964; Schmidt et al., 1958; Smith et al., 1963; Snow et al., 1978). This difficulty is reinforced by the fact that from an experimental point of view, the structure of the polymer is highly influenced by the conditions of synthesis and storage (Gunne et al., 2005). The same authors who have synthesized $(\text{C}_3\text{O}_2)_n$ that is used in this study suggest that the double bonds $\text{C}=\text{O}$ and $\text{C}=\text{C}$ are located around 1800 and 1500 cm^{-1} respectively (Gunne et al., 2005). A study of Sugimoto et al. (1986) confirm the presence of $\text{C}=\text{O}$ double bonds around 1750 cm^{-1} , and another study on the IR spectrum of the molecule C_3O_2 (Miller and Fateley, 1964) has identified the signature at 1573 cm^{-1} as being due to the $\text{C}=\text{C}$ double bond.

The spectra before and after flight of a flight exposed sample are compared in Fig. 25. The post-flight IR spectrum shows a decrease of intensity for the broad band between 3700 and 2000 cm^{-1} , and no new band appears in this spectral region. In the spectral range below 1700 cm^{-1} the evolution of the spectrum is more surprising: increase in the intensity of some bands and appearance of a band around 1060 cm^{-1} (the same band was found on the 2nd exposed sample). Without being able to be affirmative, these developments could be attributed to the formation of new bond C-O (ether, alcohol) or $\text{C}=\text{O}$, and a structural rearrangement of the polymer. We chose to limit the quantification of the disappearance of the polymer in the region between 3700 and 2000 cm^{-1} , while recognizing the limitations of these measurements given the behavior of the spectrum at lower wavenumbers.

The results of quantitative analysis are presented in Table 11. Both flight exposed samples show an evident decrease in the area of the band (3700–2000 cm^{-1}) due to photolysis. A dark control

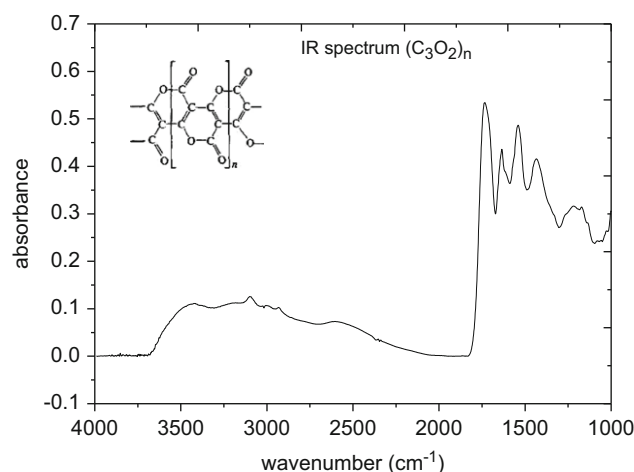


Fig. 24. IR spectrum of solid $(\text{C}_3\text{O}_2)_n$ in the region 4000–1000 cm^{-1} .

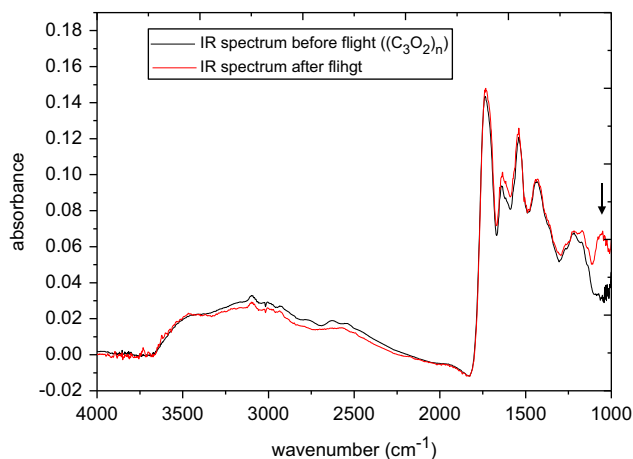


Fig. 25. Comparison of the two IR spectra before and after flight of an exposed sample of poly C₃O₂ in the region (4000–1000 cm⁻¹). A new band (1060 cm⁻¹) appears on the post-flight spectrum (shown by the arrow), the area between 3700 and 2000 cm⁻¹ are integrated for analysis.

Table 11

IR analysis results of (C₃O₂)_n (3700–2000 cm⁻¹).

CELL No. nature	Description	Band area (cm ⁻¹) (3700–2000 cm ⁻¹) before/after	Variation (%)
C ₃ O ₂ _Poly_01	Exposed	14.7/12.5	-14
C ₃ O ₂ _Poly_02	Exposed	32.1/28.7	-11
C ₃ O ₂ _Poly_03	Not exposed	17.9/18.4	+3
C ₃ O ₂ _Poly_04	Not exposed	18.8/19.1	+1
C ₃ O ₂ _Poly_05	REF, lab	12.5/13.2	+6
C ₃ O ₂ _Poly_06	REF, lab	49.9/52.9	+6

sample presents a slight increase (3%) of the area of the band, but this is probably not significant because it is close to the level of uncertainty of our measurements. But more surprising, the area of the two ground control samples increases significantly (6%). We attribute this result to the fact that ground controls may have been in contact during the storage with moisture in the air on several occasions due to sealing problems. The polyC₃O₂ is highly hygroscopic in contact with moisture, the polymer structure could change. This could be the reason for the results of the ground control samples. Since flight exposed samples and dark control samples do not present such a significant (> 3%) increase of the infrared band area, we assume that exposure to moisture happened during the storage on the ground and not during the sample preparation in the glove box.

Considering these results, the rate of photodestruction (*J*) for polyC₃O₂ is estimated to be $1.3 \pm 0.9 \times 10^{-6} \text{ s}^{-1}$ (Fig. 26). In addition to the general behavior of the spectrum that we have not yet been able to interpret, the large uncertainty (~69%) is also due to the fact that the samples are polyC₃O₂ deposited by evaporation method. The films obtained are not as homogeneous as those obtained by the sublimation method, which means that the molecules are not evenly photolyzed. Moreover, only one band has been considered for calculation (only 4 points to linear regression), which also increases the uncertainty.

3.1.5. HCN polymer

HCN polymers are dusty black solids. The films are, as for polyC₃O₂, prepared with the method of evaporation. An IR spectrum of a film of (HCN)_n (just after being prepared) is shown in Fig. 27. Their structure is still poorly known. The IR spectrum contains several bands related to amine functions (-NH₂ or -NH)

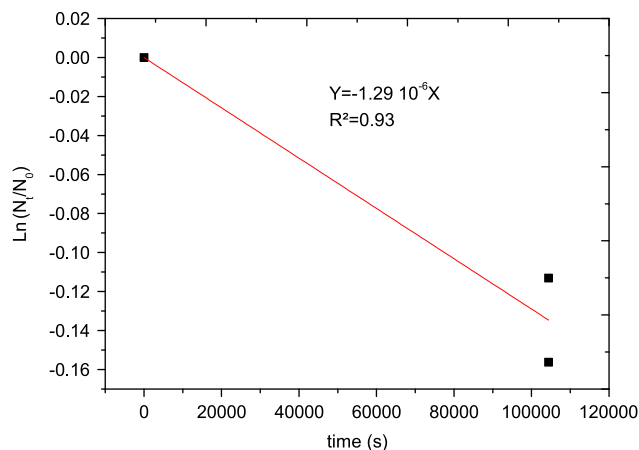


Fig. 26. Photodestruction of polyC₃O₂, variation of the abundance of material as a function of time. The Y-axis is the logarithm of the abundance of material, initial abundance *N*₀, *N*_{*t*} final abundance.

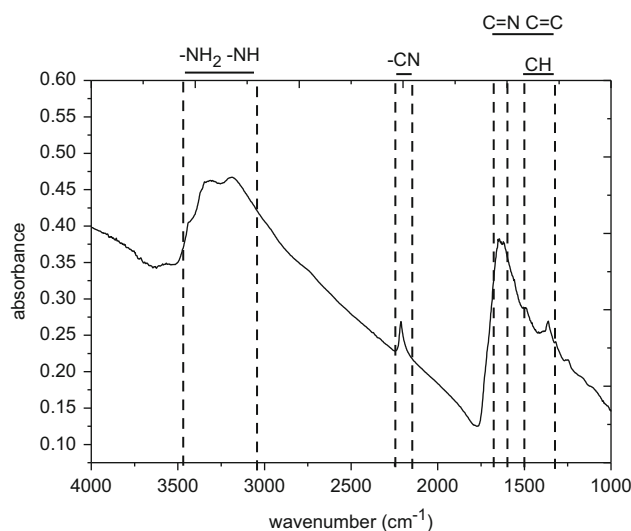


Fig. 27. IR spectrum and assignment of bands of polyHCN solid film in the region (4000–1000 cm⁻¹).

(between 3400 and 3200 cm⁻¹), nitrile (C≡N) (around 2200 cm⁻¹), C=N and C=C (1650–1360 cm⁻¹) (Imanaka et al., 2004; Quirico et al., 2008). The absence of bands around 2900 cm⁻¹ suggests the absence of CH₂ or CH₃ group. However, the presence of two peaks at 1490 and 1364 cm⁻¹ could be the signature of C–CH₃ bond, this assignment is to be confirmed.

The comparisons of spectra before and after the flight for both flight exposed, not exposed and ground reference are presented in Figs. 28–30.

These three figures representing respectively a flight exposed, a dark control and a ground control, show the same trend: the entire IR spectrum does not vary in the same way depending on the wavenumber. If some spectral characteristics remain unchanged during the experiment, the band of the triple bond C≡N (around 2200 cm⁻¹) shows a significant decrease over time. Quantifying the area of this band is not interfered by other adjoining bands. It will be used for quantitative analysis and the results are presented in Table 12.

The results of PolyHCN show that the destruction of the CN band for the 2 flight exposed samples is approximately 20% and 10% for the 2 dark control samples and little change (~5%) for the 2 ground controls kept in the laboratory. From these results, we suggest that

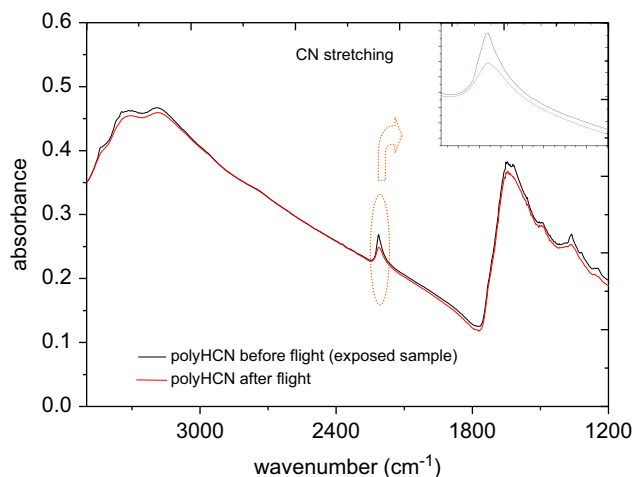


Fig. 28. Comparison of spectra before and after flight of a flight exposed polyHCN.

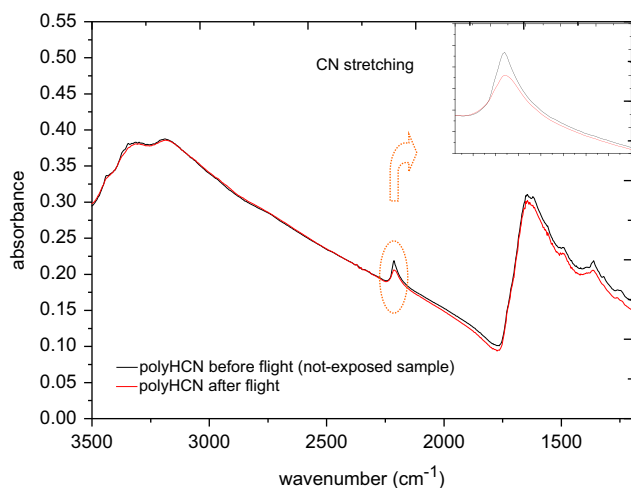


Fig. 29. Comparison of spectra before and after flight of a flight not-exposed polyHCN.

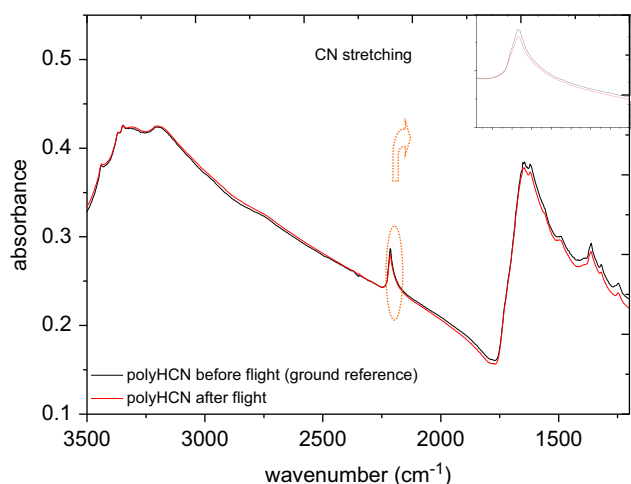


Fig. 30. Comparison of spectra before and after flight of a ground reference polyHCN.

the thermal degradation caused the destruction of approximately 10% of the CN. Several studies in LISA showed that HCN polymer is thermally unstable and can be degraded from a few tens of degrees Celsius (Le Roy, 2008). Temperatures recording of the Uvolution

Table 12
The quantitative analysis of IR spectrum for HCN polymer samples (CN stretching band), 2 cells for each category of samples.

CELL No. nature	Description	Bande area 1 (cm ⁻¹) (2256–2100 cm ⁻¹) before/after	Variation (%)
HCN_poly_01	Exposed	1.75/1.41	-19
HCN_poly_02	Exposed	1.73/1.41	-18
HCN_poly_03	Not exposed	1.44/1.27	-11
HCN_poly_04	Not exposed	1.64/1.48	-10
HCN_poly_05	REF, lab	0.84/0.80	-5
HCN_poly_06	REF, lab	1.47/1.37	-7

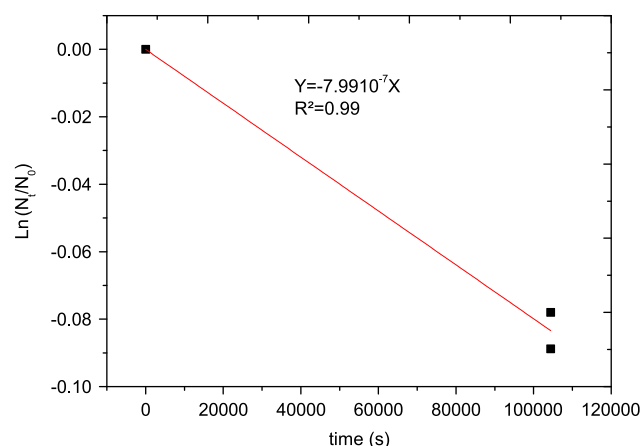


Fig. 31. Linear regression of the photodestruction of polyHCN as a function of time, the Y-axis represents the logarithm of the abundance of material, initial abundance N_0 , N_t final abundance (the thermal effect is subtracted in this linear regression).

mission show that shortly just before the launch, the temperature has exceeded 30 °C. It is likely that the polymer has begun to degrade (thermally) at that time. The variation of 20% measured for samples exposed is the sum of the thermal degradation and UV photolysis.

The rate of photodestruction (J) for polyHCN can be estimated by subtracting the effects of thermal variations for the flight samples (Table 12). J is equal to the slope of the linear regression ($J = 8.0 \pm 2.2 \times 10^{-7} \text{ s}^{-1}$) (Fig. 31).

3.1.6. Summary of the results of the space experiment

The photodestruction rates at 1 AU that we have measured for these 8 molecules thanks to the Uvolution space experiment are summarized in Table 13. The half-lives of these organic compounds is presented.

These results can be extrapolated to other astrophysical environments such as the diffuse interstellar medium and dense molecular clouds by rescaling the photon flux (UV). But as we mentioned in Section 2.1, we have no direct measurement of the solar flux (no solar spectrum provided, only data available: total photon flux equal to 29 ± 4.35 solar constant hour). In this study, for any comparison of results which require comparisons of photon flux, we use (Thuillier et al., 2004), with $I = 1.03 \times 10^{13} \text{ ph cm}^{-2} \text{ s}^{-1}$ at 1 AU (for $\lambda < 200 \text{ nm}$). For the interstellar medium (ISM), the photon flux is estimated: $I = 10^8 \text{ ph cm}^{-2} \text{ s}^{-1}$ (Mathis et al., 1983) (for $\lambda < 200 \text{ nm}$), and for dense molecular clouds (Cloud IS), we consider that the photon flux is about $10^3 \text{ ph cm}^{-2} \text{ s}^{-1}$ (Prasad and Tarafdar, 1983, p. 210) (for $\lambda < 200 \text{ nm}$).

Thus the results extrapolated to both astrophysical environments cited above are presented in Table 14. These results are only rough estimates giving an order of magnitude of half-lives

Table 13
Summary of the photodestruction rates (s^{-1}) and half-life time (day) at 1 AU measured thanks to the UVolution space experiment.

Molecule	J (s^{-1})	$t_{1/2}$ at 1 AU (day)
Glycine	$1.0 \pm 0.1 \times 10^{-06}$	8
Adenine	$< 1.9 \times 10^{-07a}$	> 41
Guanine	$< 1.9 \times 10^{-07a}$	> 41
Xanthine	$5 \pm 1 \times 10^{-07}$	16
Hypoxanthine	$< 1.9 \times 10^{-07a}$	> 41
Urea	$< 1.9 \times 10^{-07a}$	> 41
PolyC ₃ O ₂	$1.3 \pm 0.9 \times 10^{-06}$	6
PolyHCN	$8.0 \pm 2.2 \times 10^{-07}$	10

^a The upper limit is set for a variation of 2% which is the measurement uncertainty.

Table 14
Comparisons of lifetime in different astronomical regions.

Molecule	$t_{1/2}$ at A.U (days)	$t_{1/2}$ ISM (years)	$t_{1/2}$ IS cloud (years)
Glycine	8	2185	$2 \times 10^{+08}$
Adenine	> 41	> 11,570	$> 10^{+09}$
Guanine	> 41	> 11,570	$> 10^{+09}$
Xanthine	16	4553	$5 \times 10^{+08}$
Hypoxanthine	> 41	> 11,570	$> 10^{+09}$
Urea	> 41	> 11,570	$> 10^{+09}$
PolyC ₃ O ₂	6	1755	$2 \times 10^{+08}$
PolyHCN	10	2834	$3 \times 10^{+08}$

($t_{1/2}$) of these various compounds. Only the ratio of photon flux is taken into account for this extrapolation, and not the shape of UV spectra which are different in these different astrophysical environments.

3.2. Laboratory simulation

Experimental simulations have been conducted in the laboratory to be compared with the results measured in Earth orbit. These comparisons allow us to understand the extent to which kinetics traditionally measured in the laboratory can be extrapolated to space conditions. First, we present the measurements of the flux of the UV lamp, and then the results of photodissociation experiments (J) (laboratory) for the various compounds studied. The duration of exposure to UV lamp vary between different molecules, it depends on the nature of the molecule.

3.2.1. Lamp flux measurement

The photon flux of the H₂/He UV lamp is measured by N₂O actinometry (Cottin et al., 2000; Okabe, 1978). The N₂O photolysis can be described as



During the actinometry experiments, the pyrex reactor (cf. Fig. 2) is initially filled with 0.7 mbar of N₂O, and the pressure increase is followed as it is directly related to the UV flux of our lamp according to

$$f_{H_2} = \frac{VN}{\Phi RTAS} \times \frac{\partial P}{\partial t} \quad (6)$$

In which f_{H_2} is the photon flux (ph cm⁻² s⁻¹), V the volume of the reactor (0.285 L), and N , Avogadro's number= 6.02×10^{23} and $\partial P/\partial t$ the rate of variation of gas pressure inside the reactor, $\Phi=0.58 \pm 0.15$ the yield of molecule production, $R=0.082$ atm L mol⁻¹ k⁻¹, $T=298$ K the temperature inside the reactor, $A=0.42$ the absorbed fraction of UV radiation in the reactor, and $S=18.09$ cm² the surface of the irradiation rayon (at the level of photolysis).

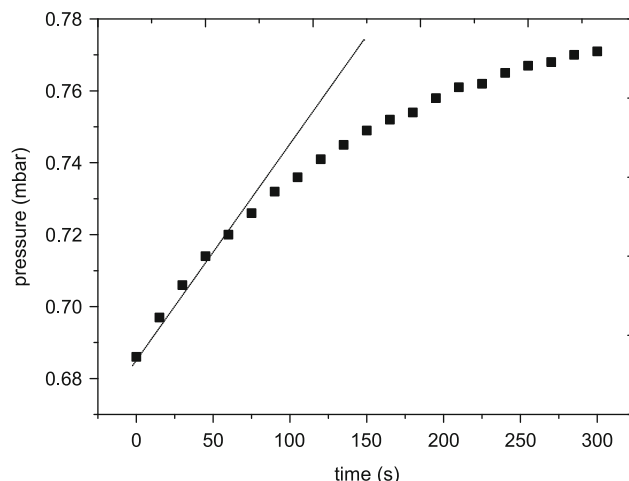


Fig. 32. Example of an actinometry experiment, evolution of pressure as a function of irradiation time. The pressure shown is subtracted from a background (evolution of pressure in the same reactor without any photolysis).

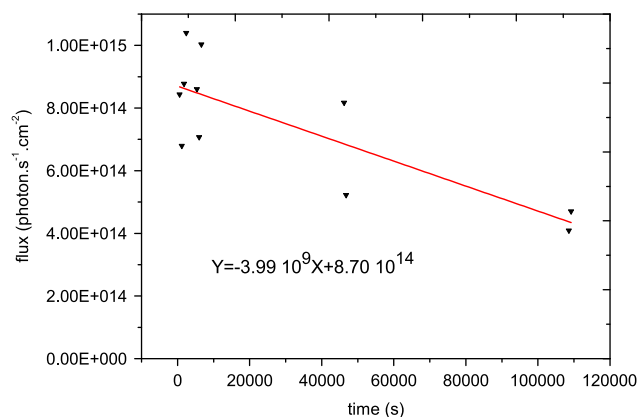


Fig. 33. Photon flux as a function of time (H₂/He UV lamp).

A typical curve of pressure variation as a function of photolysis time during these experiments is shown in Fig. 32.

It is observed that the pressure increases rapidly at first, before slowing down. Except from the general decline in flows on long-term (Fig. 33), this phenomenon can be explained by two facts (Cottin, 1999): oxygen formed during the reaction (Eq. (4)) contributes quickly in a non-negligible absorption of the UV photons. Moreover, the products (NO and O₂) from the photolysis of N₂O can also be photolyzed, which makes the reaction system quite complex. Only the first measurement has been considered for the calculation of the photon flux, because, at the beginning of an experiment, we can consider that only N₂O is absorbing photons.

This type of measurement is performed periodically and especially before each series of photolysis experiments in the laboratory. In Fig. 33 we present the lamp flux as a function of the cumulative time of lamp usage. The flux tends to decrease gradually as the lamp is ageing. Indeed, over long periods of use, color centers are formed within the crystalline structure of MgF₂, which deteriorates the optical property of the MgF₂ window.

The different flux for each photolysis experiment are calculated from the linear regression equation of Fig. 33. These relatively dispersed results generate large uncertainties (Table 15).

The results have a relatively large uncertainty. It is difficult to obtain a good estimate of the flux for that kind of UV lamps. This

Table 15

Summary of the photon flux in the laboratory for at the time of the experiment for each compound.

Molecules	Photon flux (ph cm ⁻² s ⁻¹)	Relative error (%)
Glycine	8.63 × 10 ¹⁴	35
Adenine	6.70 × 10 ¹⁴	45
Guanine	7.10 × 10 ¹⁴	43
Xanthine	8.42 × 10 ¹⁴	36
Hypoxanthine	1.91 × 10 ¹⁴	51
Urea	1.95 × 10 ¹⁴	51
PolyC ₃ O ₂	1.37 × 10 ¹⁴	72
PolyHCN	1.98 × 10 ¹⁴	50

Table 16

Evolution of the area of the two IR bands of glycine as a function of the time of photolysis.

Photolysis time (s)	Area of band 1 (3400–1900) cm ⁻¹	Variation (compared to the initial area) (%)	Area of band 2 (1800–1200) cm ⁻¹	Variation (compared to the initial area) (%)
0	102.24	0	45.04	0
3600	101.11	-2	43.57	-3
7200	96.33	-6	41.96	-7
10,800	93.75	-8	40.83	-9
14,400	89.95	-12	39.35	-13
18,000	87.72	-14	38.3	-15
25,200	83.5	-18	36.24	-20

is the main factor of uncertainty in our laboratory results (see Table 17). The plasma of the UV lamp is very sensitive to the position of the electrodes in the microwave cavity, which can result in different flux from one measurement to another.

With this measured flux, we can estimate the photolysis time necessary to simulate at least the equivalent of the solar flux (in terms of quantity of photons) during the 12 days of Earth orbit flight for exposed samples: typically 2 h.

In the laboratory, photolysis can be monitored as a function of time: we follow periodically the evolution of samples by infrared analysis. The photodissociation rates (*J*) and the half-life (*t*_{1/2}) can then be obtained with more precision than during experiments in Earth orbit (only two measurements possible). The analytical methods are the same as for samples of the space experiment (identification bands, area integration of the same bands etc.).

3.2.2. Glycine

A sample was prepared in the same conditions than samples for the space experiment. Photolysis in the laboratory was carried out during 7 h, 6 IR measurements were made and for each measurement, the same two spectral regions than for flight samples were chosen: the region between 3400 and 1900 cm⁻¹ and the region between 1800 and 1200 cm⁻¹ (see Section 3.1.1). The results are presented in Table 16.

Both integrated regions follow a similar variation that is consistent with the results of flight samples exposed on Earth orbit.

Fig. 34 shows that ln(*N*/*N*₀) is a linear function of photolysis time, the assumption of order 1 is confirmed. The slope is equal to -*J*. So *J* = 8.6 ± 0.7 × 10⁻⁶ s⁻¹. Here the uncertainty is also determined by linear regression method.

3.2.3. Purine molecules (xanthine, hypoxanthine, adenine and guanine)

The purine molecules (nitrogenous bases) are more resistant than amino acids to Solar UV. Their photolysis times in laboratory are longer than for glycine: between 9 and 15 h. The evolution of

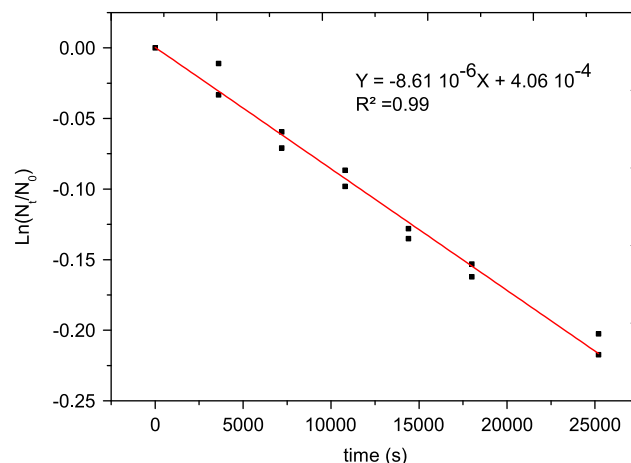


Fig. 34. Photolysis of glycine with a UV lamp H₂/He as a function of time. The Y-axis is the logarithm of the abundance of material, initial abundance *N*₀, *N*_t final abundance.

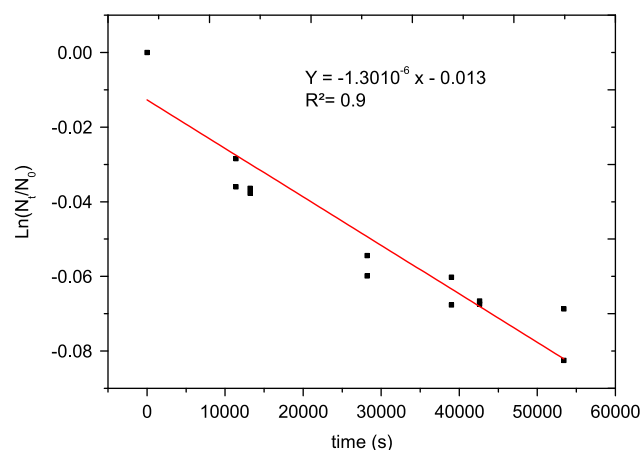


Fig. 35. Photolysis of xanthine with a UV lamp H₂/He as a function of time. The Y-axis is the logarithm of the abundance of material, initial abundance *N*₀, *N*_t final abundance *N*_t.

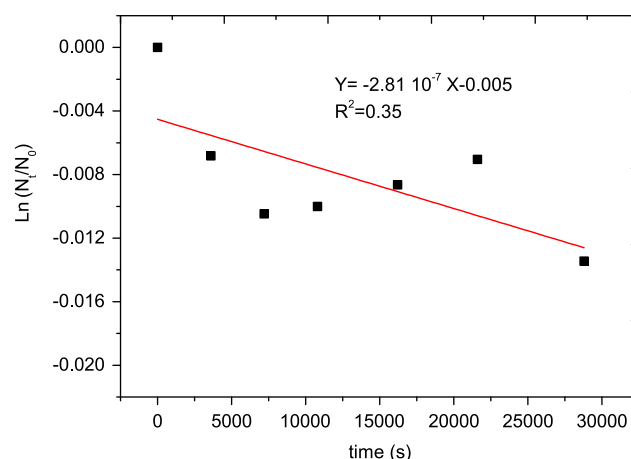


Fig. 36. Photolysis of hypoxanthine with a UV lamp H₂/He as a function of time. The Y-axis is the logarithm of the abundance of material, initial abundance *N*₀, *N*_t final abundance *N*_t.

their abundance versus the photolysis time for each of these 4 molecules is presented in Figs. 35–38, respectively, for xanthine, hypoxanthine, adenine and guanine.

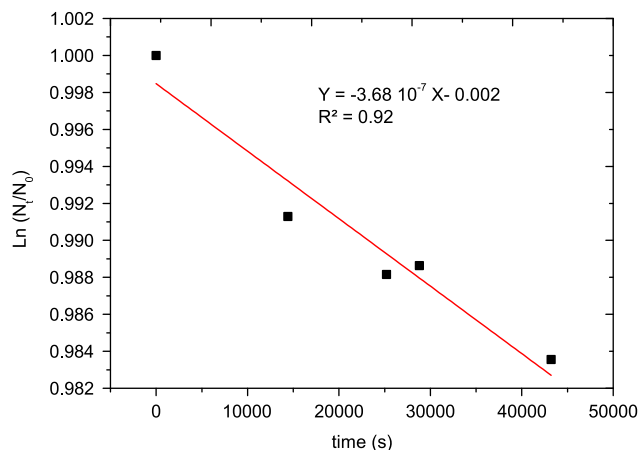


Fig. 37. Photolysis of adenine with a UV lamp H₂/He as a function of time. The Y-axis is the logarithm of the abundance of material, initial abundance N₀, final abundance N_t.

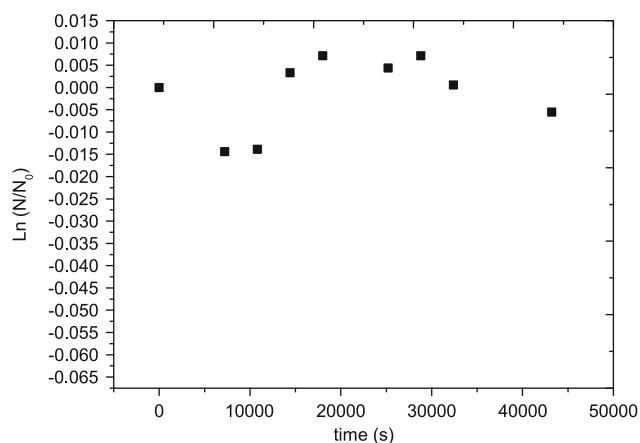


Fig. 38. Photolysis of guanine with a UV lamp H₂/He as a function of time. The Y-axis is the logarithm of the abundance of material, initial abundance N₀, N_t final abundance.

Table 17
Summary of laboratory photolysis results (photodissociation rate and half-life).

Molecule	J (s ⁻¹)	$t_{1/2}$ in laboratory (days)
Glycine	$8.6 \pm 0.7 \times 10^{-06}$	1
Adenine	$3.7 \pm 1.7 \times 10^{-07}$	23
Guanine	$< 4.7 \times 10^{-07}$	> 17
Xanthine	$1.30 \pm 0.3 \times 10^{-06}$	6
Hypoxanthine	$< 6.27 \times 10^{-07}$	> 13
Urea	$< 1.87 \times 10^{-06}$	> 4
PolyC ₃ O ₂	$1.3 \pm 1.0 \times 10^{-05}$	0.6
PolyHCN	$2.0 (+2.3/-2.0) \times 10^{-06}$	4

Using laboratory experimental conditions, we don't see any decrease in the abundance of guanine, the H₂/He lamp has no effect on this molecule after 14 h of photolysis. In the case of hypoxanthine, after 9 h of photolysis, the molecule present a 1.4% of loss of material (values below the experimental error attached to our measurements ($\pm 2\%$)). Although a linear regression (somewhat arbitrary considering the dispersion of experimental points) seems to give a rate of photodissociation which is significant ($J=2.8 \pm 3.4 \times 10^{-7} \text{ s}^{-1}$), this result will not be considered as valid because of the large uncertainty ($> 123\%$)

considering the 2% systematic errors. For 9 h of photolysis time, the upper limit of measurable J is equal to $6.27 \times 10^{-7} \text{ s}^{-1}$.

The linear regression of Fig. 38 shows that the rate of photodissociation for adenine is $3.7 \pm 1.7 \times 10^{-7} \text{ s}^{-1}$. This result is very close to the upper limit of J ($4.7 \times 10^{-7} \text{ s}^{-1}$) for 12 h photolysis. It is therefore to be considered with caution.

Finally for xanthine, J deduced from Fig. 35 is equal to $1.3 \pm 0.3 \times 10^{-6} \text{ s}^{-1}$ (for an upper limit of $3.78 \times 10^{-7} \text{ s}^{-1}$), which is consistent with the results of these molecules in the experiment in Earth orbit where only xanthine has a significant rate of photodissociation (see the results for all molecules studied in Table 17).

3.2.4. Urea

After 4 h of photolysis in the laboratory, we did not measure any loss of material (Fig. 39). Either the molecule is effectively resistant to UV light produced by the lamp, either photolysis of urea in the laboratory faces the same problem as photolysis performed in orbit: the samples are too thick, the IR spectra have the same characteristics as those used in experiment in orbit (see Section 3.1.3, Fig. 21).

3.2.5. C₃O₂ polymer ((C₃O₂)_n)

3.5 h of photolysis of C₃O₂ polymer enables us to obtain a result shown in Fig. 40, where $J=1.3 \pm 0.9 \times 10^{-5} \text{ s}^{-1}$.

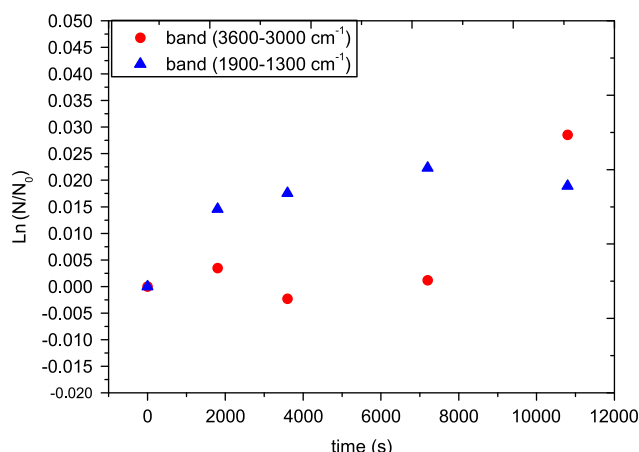


Fig. 39. Photolysis of urea with a H₂/He UV lamp as a function of time. The Y-axis is the logarithm of the abundance of material, N₀, initial abundance, N_t, final abundance. Two IR bands of urea are analyzed, neither can predict a loss of material.

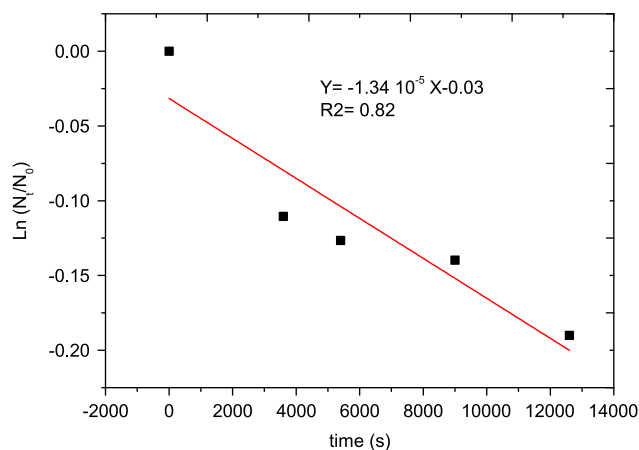


Fig. 40. Photolysis of C₃O₂ polymer with a H₂/He UV lamp as a function of time. The Y-axis is the logarithm of the abundance of material, initial abundance N₀, N_t final abundance.

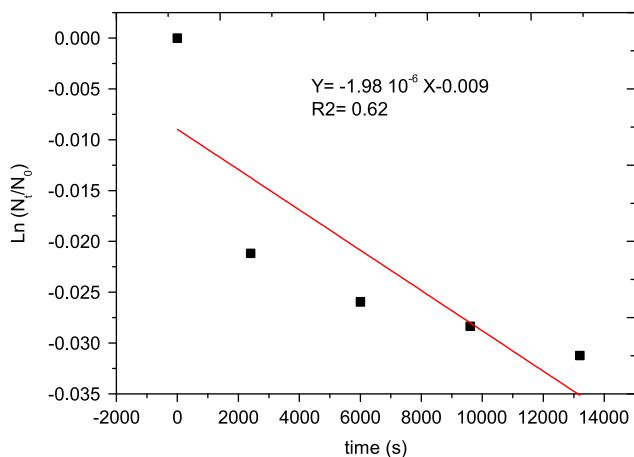


Fig. 41. Photolysis of polyHCN with a H₂/He lamp. abscissa: time of photolysis (s), ordinate ln(N/N₀): evolution in the abundance reflected on the logarithm of area normalized by the initial area.

3.2.6. PolyHCN ((HCN)_n)

The duration of photolysis for polyHCN is also 3.5 h, the quantitative analysis are still using the CN-band (CN stretching around 2200 cm⁻¹) (cf. IR spectrum in Fig. 27), the measured J is equal to $2 (+2.3/-2.0) \times 10^{-6} \text{ s}^{-1}$ (Fig. 41).

3.2.7. Summary of the laboratory simulation results

The photodissociation rates (J) are calculated and summarized in Table 17. The uncertainties are unsatisfactory, improvements are mandatory on the flux measurements and on the stability of plasma in the UV lamp (using a surfatron instead of the current cavity). These results will now be compared with results obtained in Earth orbit.

4. Comparison and discussion of the space results and the laboratory's results

At this stage, two sets of data are available, and have to be compared: the kinetics measured in space and in the laboratory. The emission spectra of our UV lamp and of the Sun are not identical, both in term of flux intensity and in term of emission spectrum. Hence the photodestruction rates measured in the laboratory cannot be directly compared to the ones determined from the UVolution space experiment. As $J = \int_{\lambda} \sigma_{\lambda}^{abs} \phi_{\lambda} I_{\lambda} d\lambda$, scaling the measurements in the laboratory to the solar flux requires assumptions to be made about the emission spectrum of the laboratory lamp, and about the absorption properties of the molecule in the VUV (for which we do not have measurements due to the lack of data in the literature).

As no absolute solar spectrum measurement is provided during the experiment, literature data (Thuillier et al., 2004) are used as a solar spectrum reference for our analysis, in a low solar activity period which was the case in 2007. The solar spectrum in the VUV region (110–200 nm) is shown in Fig. 42. The spectrum is dominated by the Lyman α band at 121.6 nm.

As a first approximation, we consider that our lamp is a monochromatic emitter at Lyman α , then $J_{lab} = \sigma_{Ly\alpha}^{abs} \Phi_{Ly\alpha} I_{Ly\alpha}^{lab}$, we also consider that the contribution of other wavelengths in space is negligible for photolytic processes: $J_{space} = \int_{\lambda} \sigma_{\lambda}^{abs} \phi_{\lambda} I_{\lambda}^{space} d\lambda$, with, and $\sigma_{\lambda}^{abs} \Phi_{\lambda} I_{\lambda}^{space} \ll \sigma_{Ly\alpha}^{abs} \Phi_{Ly\alpha} I_{Ly\alpha}^{space}$ for $\lambda \neq Ly\alpha$ (either due to a low absorption cross section, a low quantum yield or the low value of the solar flux in the VUV at $\lambda \neq Ly\alpha$), hence $J_{space} = \sigma_{Ly\alpha}^{abs} \Phi_{Ly\alpha} I_{Ly\alpha}^{space}$.

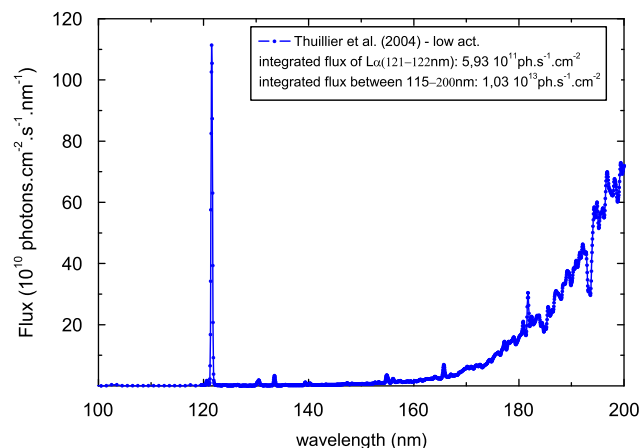


Fig. 42. Solar spectrum in VUV region (< 200 nm), the emission band at 121.6 nm is the Lyman α band which integrated area (flux) is $5.93 \times 10^{11} \text{ ph s}^{-1} \text{ cm}^{-2}$. The integrated area between 115 and 200 nm is $1.03 \times 10^{13} \text{ ph s}^{-1} \text{ cm}^{-2}$.

Then the extrapolation of the laboratory value to space is $J_{lab \rightarrow space}^{Ly\alpha} = J_{lab} \times I_{Ly\alpha}^{space} / I_{Ly\alpha}^{lab}$.

From Thuillier et al. (2004), we derive the integral of photon flux of the Lyman α band, $I_{Ly\alpha}^{space} = 5.93 \times 10^{11} \text{ ph s}^{-1} \text{ cm}^{-2}$. $I_{Ly\alpha}^{lab}$ is calculated from Fig. 33 for the time during which the laboratory experiment is carried out. In the case of glycine, $I_{Ly\alpha}^{space} / I_{Ly\alpha}^{lab} = 6.87 \times 10^{-4}$ and $J_{space} / J_{lab \rightarrow space}^{Ly\alpha} = 167$. Comparison between J_{space} and $J_{lab \rightarrow space}^{Ly\alpha}$ for each molecule is shown in Table 18.

This first approximation is limited by the fact that we have no actual measurements of our lamp emission spectrum (our hypothesis that it is a monochromatic emission is based on Table III-1, p. 112, in Okabe (1978) and is probably very sensitive to experimental conditions such as pressure, nature of the microwave cavity, H₂/He ratio) and also no measurement of the absorption spectra of the molecules in the VUV. This hypothesis results in a lower limit of $J_{lab \rightarrow space}$ derived from the calculation.

As a second approximation, we consider that our lamp is simulating the shape of the Solar UVs in the 115–200 nm domains. Then $J_{lab} = \int_{\lambda} \sigma_{\lambda}^{abs} \phi_{\lambda} I_{\lambda}^{lab} d\lambda$ and $J_{space} = \int_{\lambda} \sigma_{\lambda}^{abs} \phi_{\lambda} I_{\lambda}^{space} d\lambda$, with $\alpha \int_{\lambda} I_{\lambda}^{lab} d\lambda = \int_{\lambda} I_{\lambda}^{space} d\lambda$, $\int_{\lambda} I_{\lambda}^{lab} d\lambda$ being calculated again from Fig. 33 for the time at which the laboratory experiment is carried out and $\int_{\lambda} I_{\lambda}^{space} d\lambda = 1.03 \times 10^{13} \text{ ph s}^{-1} \text{ cm}^{-2}$ calculated from Thuillier et al. (2004). Then $J_{lab \rightarrow space}^{115-200} = J_{lab} \times \alpha$. In the case of glycine, $\alpha = 1.19 \times 10^{-2}$ and $J_{space} / J_{lab \rightarrow space}^{115-200} = 10$. Comparison between J_{space} and $J_{lab \rightarrow space}^{115-200}$ for each molecule is shown in Table 18. Differences between space and laboratory measurements in this case are smaller, and results might then look better. But as for the first approximation, this second one is also strongly dependent on the assumptions we make. 115 nm is the MgF₂ transmission cutoff and then a reasonable integration starting point. But the 200 nm limit is purely arbitrary, due to the lack of VUV measurements in the literature. The fact that the ratio between space and laboratory results is in each case > 1 is an indication that most probably photolysis occurs at $\lambda > 200 \text{ nm}$. Other ratios between space and laboratory measurements could be arbitrarily calculated. This should be confronted to real measurements of absorption spectra of each compound in the VUV, and photolysis quantum yields. Such investigations will be the subject of future studies.

Our results show that there is no easy way to extrapolate laboratory photolysis measurements to space, since the lamps cannot accurately reproduce the solar emission spectrum in the VUV. To do

Table 18

Comparisons between J measured in space and in the laboratory. The first two columns are results of measurements, the 3rd column gives values of the J measured in the laboratory extrapolated to space conditions using the 1st hypothesis and the next column is the ratio calculated for this first hypothesis. The 5th column gives values of the J measured in the laboratory extrapolated to space conditions using the 2nd hypothesis. The last column is the ratio calculated for this second hypothesis.

Molecule	J_{space} (ph cm ⁻² s ⁻¹)	J_{lab} (ph cm ⁻² s ⁻¹)	J_{lab}^{lyz}/J_{space} (ph cm ⁻² s ⁻¹)	J_{space}/J_{lab}^{lyz}	$J_{lab}^{15-200}/J_{space}$ (ph cm ⁻² s ⁻¹)	$J_{space}/J_{lab}^{15-200}$
Glycine	1.0×10^{-6}	8.6×10^{-6}	5.9×10^{-9}	175	1.0×10^{-7}	10
Adenine	$< 1.9 \times 10^{-7}$	3.7×10^{-7}	1.1×10^{-9}	≤ 169	1.9×10^{-8}	≤ 9
Guanine	$< 1.9 \times 10^{-7}$	$< 4.7 \times 10^{-7}$	$< 1.4 \times 10^{-9}$	Not significant	$< 2.5 \times 10^{-8}$	Not significant
Xanthine	5×10^{-7}	1.30×10^{-6}	4.0×10^{-9}	123	7.0×10^{-8}	7
Hypoxanthine	$< 1.9 \times 10^{-7}$	$< 6.27 \times 10^{-7}$	$< 1.9 \times 10^{-9}$	Not significant	$< 3.3 \times 10^{-8}$	Not significant
Urea	$< 1.9 \times 10^{-7}$	$< 1.87 \times 10^{-6}$	$< 5.7 \times 10^{-9}$	Not significant	$< 9.9 \times 10^{-8}$	Not significant
PolyC ₃ O ₂	1.3×10^{-6}	1.3×10^{-5}	1.1×10^{-8}	115	3.0×10^{-7}	7
PolyHCN	8×10^{-7}	2.0×10^{-6}	1.8×10^{-9}	455	3.0×10^{-8}	26

so, the absorption spectra in the VUV of each molecule should be measured, as well as the quantum yield of their destruction. This last measurement is especially difficult and requires monochromatic sources with well constrained fluxes. Subsequently both results have to be convoluted and scaled to the solar spectrum. Synchrotron sources can also be used, but only on a very limited surface of exposed material, thus compromising accurate evaluation of the effect of photolysis. On the other hand, UV light reaching low Earth orbit (at the altitude of the FOTON satellite and the Interstellar Space Station) is unfiltered. Therefore, with experiments conducted in space, many samples can be exposed simultaneously, and the measurements reflect the real solar UV spectrum, and can be extrapolated to various astrophysical environments.

5. Comparison with previous results

We now compare our results with those available in the literature. In previous Biopan missions, amino acids (alone or mixed with minerals) and PAHs were exposed under conditions similar to UVolution. In particular, Barbier et al. (2002) measured for glycine that 16% of material was destroyed after 27.4 h of direct exposure in 1997. From this result, we can calculate the $J=1.82 \times 10^{-6} \text{ s}^{-1}$, the half-life $t_{1/2}=106 \text{ h}$ (no error bars are given in the publications, quantification was performed using liquid chromatography (HPLC)). This is comparable with our results ($J=1.0 \pm 0.1 \times 10^{-6} \text{ s}^{-1}$, $t_{1/2}=186 \pm 24 \text{ h}$). Our measurement seems more reliable because our films are homogeneous, unlike those exposed in 1997, prepared by an evaporative method (of a solution of glycine).

Some molecules (adenine, guanine, xanthine and hypoxanthine) that we have selected are not destroyed by solar UV (or in a very limited amount), after 30 h of photolysis. Such duration is not enough to study the photostability of these molecules. (Ehrenfreund et al., 2007) had reached the same conclusion for PAH in Biopan V mission. Experiments of longer duration are required for studying the photostability of these organic molecules.

Laboratory studies on the photostability of various organic compounds were performed with different types of UV sources and physical states for samples (solid film, solid matrix, trapped in a mixture of ice, gas, etc.). (Peeters et al., 2003) calculated the J of glycine and nitrogenous bases (adenine and uracil) by conducting experiments in solid matrix of noble gas (the molecules are expected to behave as if they were in the gaseous phase). J measured in the laboratory has been extrapolated to space at 1 AU from the Sun. The half-life measured for glycine is $< 1 \text{ h}$ (1925 s) and a few hours for adenine. This estimate is far from what has been measured in our experiments in orbit ($t_{1/2}$ (gly): a 100 h and

$t_{1/2}$ (ade) > 41 days). In both cases, the organic molecules are not in the same physical states, the molecules in noble gas matrices have far fewer interactions such as Van der Waals and H-bonding, this favours the destruction of this material. The purines are more resistant to solar UV than glycine, which is coherent with the results presented in Schwell et al. (2006) where ionization energies were measured to be higher for the nitrogenous bases (adenine and purine, etc.) than for amino acids. First fragmentation for glycine was observed at 132 nm, while first fragmentation for nucleobases was observed below 107 nm (Schwell et al., 2006). But again, those data were not measured on films like our samples, but rather in the gaseous phase.

ten Kate et al. (2005) have studied the photolysis of glycine in the form of solid films in the laboratory with two UV lamps that emit at different ranges of wavelength. With a H₂ lamp (Lyman α and a large feature at 160 nm) of equivalent photon flux ($10^{14} \text{ ph cm}^{-2} \text{ s}^{-1}$), $t_{1/2}$ is of the order of the hour ($1.2 \pm 0.2 \text{ h}$), which can be compared to our laboratory results (22 h for a lamp (2% H₂ in He)). The difference of results could arise from the different spectral emission due to different gas composition of the lamp. In contrast, glycine photolyzed by a D₂ lamp (190–400 nm) has a $t_{1/2}$ 1000 times higher ($500 \pm 111 \text{ h}$). Photolysis of glycine occurs essentially in the VUV region.

6. Conclusion

The UVolution experiment in BIOPAN-6 aimed to study the photostability of organic molecules in space conditions. The cells, the samples holders, have resisted the space conditions throughout the duration of the experiment and returned safely the samples to Earth for analysis. The kinetics of photolysis of 8 organic molecules relevant to the study of meteorites and comets have been measured. The results are compared both with the results from previous LEO experiments and with laboratory simulations. We can conclude that the H₂/He lamp is not a good simulator of the solar UV spectrum ($< 200 \text{ nm}$). It is now essential to study the absorption VUV spectrum and dissociation quantum yields for each molecule as well as the emission spectra of the UV lamp.

The results have provided new data on the photostability of organic compounds in space. The half-lives at a distance from the Sun of 1 AU range from a few days to more than forty days for the most photo-resistant. Glycine, polyHCN and polyC₃O₂ are the most fragile molecules exposed, while purine molecules are more stable. This stability of purine molecules measured on films is consistent with previous measurement with gas phase compounds (Schwell et al., 2006). Longer durations of exposure are necessary to improve the measurements. Evidence is shown that laboratory VUV lamps have to be improved to better simulate to solar spectrum.

Experiments of longer duration such as AMINO and PROCESS should allow us to have results on a wider range of molecules. The two last exposure programs are implemented outside the International Space Station. The PROCESS experiment was part of the EXPOSE-E/Utah ESA exposure facility outside the Columbus module from Feb. 2008 to Aug. 2009. It was returned to Earth in Sept. 2009, and samples are currently analyzed. The AMINO experiment is part of the EXPOSE-R (ESA) facility that has been installed outside the Zvezda Russian module in February 2009 and should be returned to Earth in August 2010. PROCESS and AMINO are quite similar to UVolution (same kind of hardware and samples), except than a longer exposure time to solar UVs is expected (10–20 times more than during the Biopan-6 mission). Thus, new data should be available soon to better constrain the photostability of organic compounds in space.

BIOPAN and EXPOSE facilities are very valuable; however, these experiments suffer significant limitations that adversely impact science return:

- (1) The instruments are passive, residing outside space modules in orbit and the total integrated time of exposure to solar radiation is small compared to the total time in orbit. While nothing can be done to change the fact that the satellite or the ISS is on the night side of Earth approximately half the time, even when the exposure facility is on the day side of the Earth, it is often not pointing directly toward the Sun. For the 12-day BIOPAN 6 mission, 29 h of direct exposure were measured (10% exposure ratio); for a 1-year mission, it is estimated the EXPOSE-E and -R samples will be exposed to the Sun for an integrated duration of only 240 h (2.7% exposure ratio).
- (2) The kinetics of the evolution of the sample cannot be accurately measured. Only two measurement time points are available: the state and composition of the sample before launch, and the state and composition when it returns to the laboratory after its journey in space. Therefore, the results presented in this paper are given with rather large uncertainties.
- (3) The temperature of the samples is not controlled, limiting the selection of molecules for the experiments. For compounds that are not sufficiently refractory, sublimation can become noticeable if the sample reaches high temperatures (“high” depends on the nature of the molecule, but can be as “low” as 40 °C for long-duration experiments). Furthermore, to date it has been impossible to study the evolution of samples that must be held at low temperature (pure ice, or ice mixtures, at T in the 10–100 K range). Such experiments are both important and common in the laboratory, enhancing the understanding of chemical evolution in interstellar and cometary ices, at the surfaces of the icy satellites of the giant planets, and at the surfaces of transneptunian objects.

NASA's Ames Research Center is developing a free-flying nanosatellite, O/OREOS (Organism/Organic Exposure to Orbital Stresses), planned for launch in 2010, that addresses issue (2) above and, to a significant degree, issue (1) as well: one of the two O/OREOS payload instruments will directly monitor sample evolution resulting from UV exposure on a weekly basis in space using an integral miniaturized UV–visible–NIR spectrometer. Its orbital inclination and period will result in > 1300 h of exposure of the organic samples over a 6-months mission (30% exposure ratio). A next step will be crossed with VITRINE, a new project currently under study by CNES. VITRINE is a logical and effective way to leverage and extend such technology to platforms such as ISS, and addresses issues (1), (2), and (3) listed above.

This space instrument will be dedicated to experiments on the photochemistry of organic molecules in the solid phase (refractory

compounds or ices), or in the gas phase, for long-duration exposures with

- A ratio of exposure times relatively high, pointing to the active Sun.
- The ability to monitor samples in situ and in real time with IR and UV spectrometers onboard.
- The ability to control the sample temperature from below 100 K to room temperature. This instrument is designed for installation and operation outside the International Space Station. These projects are the next generation of exposure in orbit, and will be following the work described here (UVolution, AMINO & PROCESS).

Acknowledgements

This program has been selected by ESA in the frame of the AO Life and Physical Sciences and Applied Research Projects 2004. The authors would like to acknowledge the support of ESA (especially René Demets), CNES (especially Michel Viso for the human, financial and technical supports), COMAT aerospace (Toulouse, France) and Kayser Threde (Munich, Germany).

Professor Beck (Institut für Anorganische Chemie der Universität Bonn) kindly provided us samples of carbon suboxide polymer, and Professor Minard (Penn State Astrobiology Research Center and Department of Chemistry, Penn State University) provided us samples of HCN polymer which were used in UVolution.

We also thank Patrick Ausset (LISA) for his valuable help to characterize the thickness of the samples.

The two referees of the paper are thanked for their valuable comments to improve the manuscript.

References

- Agarwal, V.K., Schutte, W., Greenberg, J.M., Ferris, J.P., Briggs, R., Connor, S., Vandebult, C., Baas, F., 1985. Photochemical-reactions in interstellar grains photolysis of CO, NH₃, and H₂O. *Origins of Life and Evolution of the Biosphere* 16, 21–40.
- Albrecht, G., Corey, R.B., 1939. The crystal structure of glycine. *Journal of the American Chemical Society* 61, 1087–1103.
- Barbier, B., Bertrand, M., Boillot, F., Chabin, A., Chaput, D., Henin, O., Brack, A., 1998. Delivery of extraterrestrial amino acids to the primitive Earth. Exposure experiments in Earth orbit. *Biological Science in Space* 12, 92–95.
- Barbier, B., Henin, O., Boillot, F., Chabin, A., Chaput, D., Brack, A., 2002. Exposure of amino acids and derivatives in the Earth orbit. *Planetary and Space Science* 50, 353–359.
- Bernstein, M.P., Dworkin, J.P., Sandford, S.A., Cooper, G.W., Allamandola, L.J., 2002. Racemic amino acids from the ultraviolet photolysis of interstellar ice analogues. *Nature* 416, 401–403.
- Bernstein, M.P., Sandford, S.A., Allamandola, L.J., Chang, S., Scharberg, M.A., 1995. Organic-compounds produced by photolysis of realistic interstellar and cometary ice analogs containing methanol. *Astrophysical Journal* 454, 327–344.
- Biver, N., Bockelée-Morvan, D., Crovisier, J., Davies, J.K., Matthews, H.E., Wink, J.E., Rauer, H., Colom, P., Dent, W.R.F., Despois, D., Moreno, R., Paubert, G., Jewitt, D., Senay, M., 1999. Spectroscopic monitoring of comet C/1996 B2 (Hyakutake) with the JCMT and IRAM radio telescopes. *Astronomical Journal* 118, 1850–1872.
- Blake, A.R., Jennings, P.P., Eeles, W.T., 1964. Carbon suboxide polymers. I. structure of thermal polymers. *Transactions of the Faraday Society* 60, 691.
- Bockelée-Morvan, D., Lis, D.C., Wink, J.E., Despois, D., Crovisier, J., Bachiller, R., Benford, D.J., Biver, N., Colom, P., Davies, J.K., Gerard, E., Germain, B., Houde, M., Mehringer, D., Moreno, R., Paubert, G., Phillips, T.G., Rauer, H., 2000. New molecules found in comet C/1995 O1 (Hale-Bopp)—Investigating the link between cometary and interstellar material. *Astronomy & Astrophysics* 353, 1101–1114.
- Bockelée-Morvan, D., Crovisier, J., Mumma, M.J., Weaver, H.A., 2004. The composition of cometary volatiles. In: Festou, M., Keller, H.U., Weaver, H.A. (Eds.), *Comets II*. University of Arizona Press, Tucson.
- Boillot, F., Chabin, A., Bure, C., Venet, M., Belsky, A., Bertrand-Urbaniak, M., Delmas, A., Brack, A., Barbier, B., 2002. The Perseus Exobiology mission on MIR: Behaviour of amino acids and peptides in earth orbit. *Origins of Life and Evolution of the Biosphere* 32, 359–385.

- Botta, O., Bada, J.L., 2002. Extraterrestrial Organic Compounds in Meteorites. *Surveys in Geophysics* 23, 411–467.
- Cottin, H., 1999. Chimie organique de l'environnement cométaire : étude expérimentale de la contribution de la composante organique réfractaire à la phase gazeuse. astronomie et astrophysique Université Paris XII.
- Cottin, H., Coll, P., Coscia, D., Fray, N., Guan, Y.Y., Macari, F., Raulin, F., Rivron, C., Stalport, F., Szopa, C., Chaput, D., Viso, M., Bertrand, M., Chabin, A., Thirkell, L., Westall, F., Brack, A., 2008. Heterogeneous solid/gas chemistry of organic compounds related to comets, meteorites, Titan, and Mars: laboratory and in lower Earth orbit experiments. *Advances in Space Research* 42, 2019–2035.
- Cottin, H., Despois, D., 2009. Comets and astrobiology. In: Wong, J.T.-F., Lazcano, A. (Eds.), *Prebiotic Evolution and Astrobiology* Landes. Bioscience of Texas.
- Cottin, H., Fray, N., 2008. Distributed sources in comets. *Space Science Reviews* 138, 179–197.
- Cottin, H., Gazeau, M.C., Benilan, Y., Raulin, F., 2001a. Polyoxymethylene as parent molecule for the formaldehyde extended source in comet Halley. *Astrophysical Journal* 556, 417–420.
- Cottin, H., Gazeau, M.C., Doussin, J.F., Raulin, F., 2000. An experimental study of the photodegradation of polyoxymethylene at 122, 147 and 193 nm. *Journal of Photochemistry and Photobiology A—Chemistry* 135, 53–64.
- Cottin, H., Szopa, C., Moore, M.H., 2001b. Production of hexamethylenetetramine in photolyzed and irradiated interstellar cometary ice analogs. *Astrophysical Journal* 561, L139–L142.
- Cronin, J.R., 1989. Origin of organic compounds in carbonaceous chondrites. *Advances in Space Research* 9, 59–64.
- Delabar, J.M., Majoube, M., 1978. Infrared and Raman-spectroscopic study of N-15 and D-substituted Guanines. *Spectrochimica Acta Part A—Molecular and Biomolecular Spectroscopy* 34, 129–140.
- Demets, R., Schulte, W., Baglioni, P., 2005. The past, present and future of BIOPAN. *Space Life Sciences: astrobiology: Steps toward Origin of Life and Titan before Cassini* 36, 311–316.
- Ehrenfreund, P., Bernstein, M.P., Dworkin, J.P., Sandford, S.A., Allamandola, L.J., 2001. The photostability of amino acids in space. *Astrophysical Journal* 550, L95–L99.
- Ehrenfreund, P., Ruitkamp, R., Peeters, Z., Foing, B., Salama, F., Martins, Z., 2007. The ORGANICS experiment on BIOPAN V: UV and space exposure of aromatic compounds. *Planetary and Space Science* 55, 383–400.
- Elsila, J.E., Glavin, D.P., Dworkin, J.P., 2009. Cometary glycine detected in samples returned by Stardust. *Meteoritics and Planetary Science* 44, 1323–1330.
- Fernandez-Quejo, M., de la Fuente, A., Navarro, R., 2005. Theoretical calculations and vibrational study of hypoxanthine in aqueous solution. *Journal of Molecular Structure* 744, 749–757.
- Fomenkova, M.N., 1999. On the organic refractory component of cometary dust. *Space Science Reviews* 90, 109–114.
- Gerakines, P.A., Moore, M.H., 2001. Carbon suboxide in astrophysical ice analogs. *Icarus* 154, 372–380.
- Gerakines, P.A., Moore, M.H., Hudson, R.L., 2004. Ultraviolet photolysis and proton irradiation of astrophysical ice analogs containing hydrogen cyanide. *Icarus* 170, 202–213.
- Gerakines, P.A., Schutte, W.A., Ehrenfreund, P., 1996. Ultraviolet processing of interstellar ice analogs. 1. Pure ices. *Astronomy and Astrophysics* 312, 289–305.
- Gunasekaran, S., Sankari, G., Ponnusamy, S., 2005. Vibrational spectral investigation on xanthine and its derivatives-theophylline, caffeine and theobromine. *Spectrochimica Acta Part A—Molecular and Biomolecular Spectroscopy* 61, 117–127.
- Gunne, J., Beck, J., Hoffbauer, W., Krieger-Beck, P., 2005. The structure of poly(carbonsuboxide) on the atomic scale: a solid-state NMR study. *Chemistry—a European Journal* 11, 4429–4440.
- Hayatsu, R., 1964. Orgueil meteorite—organic nitrogen contents. *Science* 146, 1291–1293.
- Hayatsu, R., Studier, M.H., Moore, L.P., Anders, E., 1975. Purines and Triazines in Murchison meteorite. *Geochimica Et Cosmochimica Acta* 39, 471–488.
- Hirakawa, A.Y., Okada, H., Sasagawa, S., Tsuboi, M., 1985. Infrared and Raman spectra of Adenine and its N-15 and C-13 substitution products. *Spectrochimica Acta Part A—Molecular and Biomolecular Spectroscopy* 41, 209–216.
- Iitaka, Y., 1960. The crystal structure of beta-glycine. *Acta Crystallographica* 13, 35–45.
- Imanaka, H., Khare, B.N., Elsilá, J.E., Bakes, E.L.O., McKay, C.P., Cruikshank, D.P., Sugita, S., Matsui, T., Zare, R.N., 2004. Laboratory experiments of titan tholin formed in cold plasma at various pressures: implications for nitrogen-containing polycyclic aromatic compounds in Titan haze. *Icarus* 168, 344–366.
- Kissel, J., Krueger, F.R., 1987. The organic-component in dust from comet HALLEY as measured by the PUMA mass-spectrometer on board VEGA-1. *Nature* 326, 755–760.
- Kissel, J., Sagdeev, R.Z., Bertaux, J.L., Angarov, V.N., Audouze, J., Blamont, J.E., Buchler, K., Evlanov, E.N., Fechtig, H., Fomenkova, M.N., Vonhoerner, H., Inogamov, N.A., Khromov, V.N., Knabe, W., Krueger, F.R., Langevin, Y., Leonas, V.B., Levassurregourd, A.C., Managadze, G.G., Podkolzin, S.N., Shapiro, V.D., Tabaldyev, S.R., Zubkov, B.V., 1986. Composition of comet Halley dust particles from Vega observations. *Nature* 321, 280–282.
- Kutzelnigg, W., Mecke, R., Schrader, B., Nerdel, F., Kresse, G., 1961. Die schwingungsspektren des Harnstoff-molekuls, des Harnstoff-kristalls und des wirtsgitters der Harnstoff-Einschlussverbindungen. *Zeitschrift Fur Elektrochemie* 65, 109–119.
- Le Roy, L., 2008. Synthèse et étude de la dégradation thermique des polymères de HCN: Application aux sources distribuées de CN dans les comètes master. Université Paris XII.
- Lis, D.C., Keene, J., Young, K., Phillips, T.G., Bockelée-Morvan, D., Crovisier, J., Schilke, P., Goldsmith, P.F., Bergin, E.A., 1997. Spectroscopic observations of comet C/1996 B2 (Hyakutake) with the caltech submillimeter observatory. *Icarus* 130, 355–372.
- Liu, Z., Zhong, L., Ying, P., Feng, Z., Li, C., 2008. Crystallization of metastable beta glycine from gas phase via the sublimation of alpha or gamma form in vacuum. *Biophysical Chemistry* 132, 18–22.
- Martins, Z., Alexander, C.M.O.D., Orzechowska, G.E., Fogel, M.L., Ehrenfreund, P., 2007a. Indigenous amino acids in primitive CR meteorites. *Meteoritics and Planetary Science* 42, 2125–2136.
- Martins, Z., Botta, O., Fogel, M.L., Sephton, M.A., Glavin, D.P., Watson, J.S., Dworkin, J.P., Schwartz, A.W., Ehrenfreund, P., 2008. Extraterrestrial nucleobases in the Murchison meteorite. *Earth and Planetary Science Letters* 270, 130–136.
- Martins, Z., Hofmann, B.A., Gnos, E., Greenwood, R.C., Verchovsky, A., Franchi, I.A., Jull, A.J.T., Botta, O., Glavin, D.P., Dworkin, J.P., Ehrenfreund, P., 2007b. Amino acid composition, petrology, geochemistry, ¹⁴C terrestrial age and oxygen isotopes of the ShiÄYr 033 CR chondrite. *Meteoritics and Planetary Science* 42, 1581–1595.
- Mathis, J.S., Mezger, P.G., Panagia, N., 1983. Interstellar radiation-field and dust temperature in the diffuse interstellar matter and in giant molecular clouds. *Astronomy and Astrophysics* 128, 212–229.
- Mathlouthi, M., Seuvre, A.M., Koenig, J.L., 1984. FT-IR and laser-Raman spectra of constituents of nucleic-acids. 2. FT-IR and laser-Raman spectra of adenine and adenosine. *Carbohydrate Research* 131, 1–15.
- Miller, F.A., Fateley, W.G., 1964. The infrared spectrum of carbon suboxide. *Spectrochimica Acta* 20, 253–266.
- Okabe, H., 1978. *Photochemistry of Small Molecules*. John-Wiley & Sons, Gauthersbourg, MD.
- Peeters, Z., Botta, O., Charney, S.B., Ruitkamp, R., Ehrenfreund, P., 2003. The astrobiology of nucleobases. *Astrophysical Journal* 593, L129–L132.
- Prasad, S.S., Tarafdar, S.P., 1983. UV-radiation field inside dense clouds—its possible existence and chemical implications. *Astrophysical Journal* 267, 603–609.
- Quirico, E., Montagnac, G., Lees, V., McMillan, P.F., Szopa, C., Cernogora, G., Rouzaud, J.N., Simon, P., Bernard, J.M., Coll, P., Fray, N., Minard, R.D., Raulin, F., Reynard, B., Schmitt, B., 2008. New experimental constraints on the composition and structure of tholins. *Icarus* 198, 218–231.
- Raunier, S., Chiavassa, T., Duvernay, F., Borget, F., Aycard, J.P., Dartois, E., d'Hendecourt, L., 2004. Tentative identification of urea and formamide in ISO-SWS infrared spectra of interstellar ices. *Astronomy & Astrophysics* 416, 165–169.
- Rosado, M.T., Duarte, M.L.T.S., Fausto, R., 1998. Vibrational spectra of acid and alkaline glycine salts. *Vibrational Spectroscopy* 16, 35–54.
- Rousseau, B., Keuleers, R., Dessey, H.O., Geise, H.J., Van Alsenoy, C., 1999. Solids modeled by ab-initio crystal field methods. Effects of intermolecular interactions on the vibrational spectrum of urea. *Chemical Physics Letters* 302, 55–59.
- Sakai, H., Hosogai, H., Kawakita, T., Onuma, K., Tsukamoto, K., 1992. Transformation of alpha-glycine to gamma-glycine. *Journal of Crystal Growth* 116, 421–426.
- Sandford, S.A., Aleon, J., Alexander, C.M.O., Araki, T., Bajt, S., Baratta, G.A., Borg, J., Bradley, J.P., Brownlee, D.E., Brucato, J.R., Burchell, M.J., Busemann, H., Butterworth, A., Clemett, S.J., Cody, G., Colangeli, L., Cooper, G., D'Hendecourt, L., Djouadi, Z., Dworkin, J.P., Ferrini, G., Fleckenstein, H., Flynn, G.J., Franchi, I.A., Fries, M., Gilles, M.K., Glavin, D.P., Gounelle, M., Grossemy, F., Jacobsen, C., Keller, L.P., Kilcoyne, A.L.D., Leitner, J., Matrajt, G., Meibom, A., Mennella, V., Mostefaoui, S., Nittler, L.R., Palumbo, M.E., Papanastassiou, D.A., Robert, F., Rotundi, A., Snead, C.J., Spencer, M.K., Stadermann, F.J., Steele, A., Stephan, T., Tsou, P., Tylliszczak, T., Westphal, A.J., Wirick, S., Wopenka, B., Yabuta, H., Zare, R.N., Zolensky, M.E., 2006. Organics captured from comet 81P/Wild 2 by the Stardust spacecraft. *Science* 314, 1720–1724.
- Schmidt, L., Boehm, H.P., Hofmann, U., 1958. Über die rite kohle Von klemenc. 2. *Zeitschrift Fur Anorganische Und Allgemeine Chemie* 296, 246–261.
- Schwell, M., Jochims, H.W., Baumgartel, H., Dulieu, F., Leach, S., 2006. VUV photochemistry of small biomolecules. *Planetary and Space Science* 54, 1073–1085.
- Smith, R.N., Carter, C.C., Smith, E.N., Young, D.A., 1963. Structure and properties of carbon suboxide polymer. *Inorganic Chemistry* 2, 829.
- Snow, A.W., Haubenstock, H., Yang, N.L., 1978. Poly(carbon suboxide)—characterization, polymerization, and radical structure. *Macromolecules* 11, 77–86.
- Stalport, F., Guan, Y.Y., Coll, P., Szopa, C., Macari, F., Raulin, F., Chaput, D., Cottin, H., 2010. UV-olition, a photochemistry experiment in Low Earth Orbit: investigation of the photostability of carboxylic acids exposed to Mars surface UV radiation conditions. *Astrobiology* 10, 449–461.
- Sugimoto, S., Nishii, M., Sugiura, T., 1986. Radiation-induced chemical reactions of carbon monoxide and hydrogen mixture—IV. On the water produced by the addition of small amounts of ammonia. *International Journal of Radiation Applications and Instrumentation. Part C. Radiation Physics and Chemistry* 27, 153–155.
- ten Kate, I.L., Garry, J.R.C., Peeters, Z., Quinn, R., Foing, B., Ehrenfreund, P., 2005. Amino acid photostability on the Martian surface. *Meteoritics & Planetary Science* 40, 1185–1193.
- Thuillier, G., Floyd, L., Woods, T.N., Cebula, R., Hilsenrath, E., Herse, M., Labs, D., 2004. Solar irradiance reference spectra for two solar active levels. *Solar Variability and Climate Change* 34, 256–261.
- Uvdal, K., Bodö, P., Ihs, A., Liedberg, B., Salaneck, W.R., 1990. X-ray photoelectron and infrared spectroscopy of glycine adsorbed upon copper. *Journal of Colloid and Interface Science* 140, 207–216.
- van der Velden, W., Schwartz, A.W., 1977. Search for purines and pyrimidines in the Murchison meteorite. *Geochimica Et Cosmochimica Acta* 41, 961–968.